14 Self-Assembled Monolayers on Nanostructured Composites for Electrochemical Sensing Applications

Nada F. Atta, Ekram H. El-Ads, and Ahmed Galal

Contents

N.F. Atta • E.H. El-Ads • A. Galal (✉)
Chemistry Department, Faculty of Science, Cairo University, Giza, Egypt
e-mail: galal@sci.cu.edu.eg

M. Aliofkhazraei, A.S.H. Makhlouf (eds.), *Handbook of Nanoelectrochemistry*,
DOI 10.1007/978-3-319-15266-0_38

Abstract

Self-assembled monolayer (SAM) represents one of the methods to precisely modify surface structures in the nanoscale dimension. It has opened up a new era of exploration and has a profound impact on sensors and biosensors due to its unique properties. Different self-assemblies will be considered in this chapter: SAM of metallic nanoparticles on polymeric film, SAM of surfactant on polymeric film, and SAM of S-containing compounds on nanometallic films. The main goal of this chapter is to present comprehensive collection of the recent achievements in this area. Several issues will be discussed including the morphology, sensitivity, selectivity, stability, and electrochemical properties of the sensor.

Keywords

Nanostructured composites • Self-assembled monolayer • Conducting polymers • Metal nanoparticles • Surfactants • Sensors

General Introduction

Sensor

A sensor can be described as a device capable of converting the different types of signals. Systems generate signals due to physical, chemical, biological, and several other changes that are normally transformed into electrical signals. A typical sensor responds with selectivity and specificity to the target analyte without interference (Fig. 1). The main components of the sensor are transducer and detector devices. Signals are collected, amplified, and displayed using signal processor. A biosensor is a specific type of sensor that should include a biological component in its sensing element; an example is blood glucose biosensor. On the other hand, a chemical sensor can convert the chemical information that results from a chemical reaction including the analyte itself or from a physical property of the system under investigation into an analytically representative signal. This chemical information may be ranged from the concentration of a specific component to the analysis of the total composition of the sample. Selectivity, anti-interference ability, linear dynamic

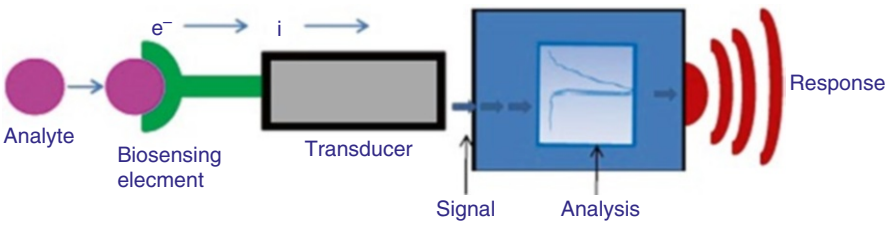

Fig. 1 A schematic of an electrochemical biosensor with electrochemical transducer (Reprinted from [1], Copyright (2013), with permission from Elsevier)

ranges, limit of detection, sensitivity, and precision of response can be used to experimentally evaluate the performance of any biosensor. Other parameters can be taken into consideration like portability, ease of use, stability, and time of response. A typical sensing surface should be renewable so that several repetitive measurements can be made [1].

Nanostructured Hybrids for Electrochemical Sensing Applications

Self-assembled monolayer (SAM), a fashionable approach to electrically orient and address a molecular component of interest, represents one of the methods that precisely modify the surface structure in the nanoscale dimension. It has opened up a new era of exploration and has a profound impact on sensors and biosensors due to its unique properties. SAM may be nanometallic film, surfactant film, or SAM of S-containing compounds, particularly cysteine over modified or bare substrates. This chapter will give a brief review of SAM of metallic nanoparticles (Pd, Pt, etc.) over different polymeric films (poly(3-methylthiophene), polypyrrole, polyfuran, etc.) showing the enhanced catalytic activity of these hybrid nanocomposites and its biosensing applications. Moreover, it will show the SAM of different surfactants over polymeric film of poly(3,4-ethylenedioxythiophene) PEDOT and over the hybrid nanocomposite of PEDOT/gold nanoparticles. It will show its biosensing applications toward different neurotransmitters and drugs. On the other hand, this chapter will explain the effect of formation of SAM of S-containing compounds on different substrates: macro- and nanoelectrode (bare electrodes and metallic nanoparticle-modified electrodes). It will display the sensing applications of gold nanoparticles electrode modified with self-assembled monolayers of cysteine and surfactants. It will explain the role of SAM of surfactant and that of cysteine in the enhancement of the catalytic activity and improvement of the stability of the proposed electrodes toward sensing applications.

Nanostructured Metallic Particles on Polymers

General Introduction

The physicochemical characteristics of bare electrodes can be improved using electrode modifiers such as conducting polymers. Conducting polymers can significantly improve the analytical detection by enhancing the sensitivity and selectivity and lowering the detection limit; therefore, they are utilized as redox mediators for several analytes. Moreover, they exhibit an anti-interference ability which resulted in electrochemical responses with excellent repeatability. On the other hand, the catalytic electrode processes can be activated using mediating agent that can be used in the solution containing the analyte, and this was the first developed system suitable for this purpose. On the other hand, the mediating agent can be immobilized directly on the electrode surface through electrochemical polymerization resulting in chemically modified electrode. The electrochemical polymerization can

be achieved via galvanostatic, potentiostatic, or potential sweeping techniques. As a result, these modified electrodes exhibited several advantages such as reduced matrix effect, fast regeneration of the catalyst, anti-contamination of the solution by the redox mediator, and improved performance of the redox mediator [2]. Due to their combination of useful electrochemical, electrochromic, and electrocatalytic properties [3]; antifouling, mechanical, optical, and electronic properties; as well as their high sensitivities and low detection limits [4], conducting polymers have been widely used for a variety of sensors, biosensors [5], and actuators to improve the response time, sensitivity, reliability, and versatility of different sensors and biosensors [6].

On the other hand, it is well known that metal nanoparticles exhibited unique electronic, physical, and chemical characteristics besides their small size (1–100 nm) and flexibility. As a result, they have obvious applications in electrochemical sensing and catalysis. Metal nanoparticles are described as "electron wires" that enhance the kinetics of electron transfer between the redox centers of the target molecules and the electrode surface [1]. It is well known that the catalytic activity of metal nanoparticles is affected by their dispersion and surface properties. Conducting polymers exhibited metallike conductivity reaching a range as high as 10^3–10^5 S cm^{-1} and long π-conjugation length; therefore, they are considered as useful matrices for metal nanoparticles immobilization [7]. In addition, the high porosity of the conducting polymer structure generates additional electrocatalytic sites by allowing the dispersion of metal nanoparticles into the polymer matrix. As well, the facilitation of the charge transfer kinetics between the substrate and the dispersed metal nanoparticles is more obvious in the conducting polymer matrix. Also, metal nanoparticles' incorporation to conducting polymers enhances the performance for both the "host" and the "guest" leading to various physical characteristics and potential applications in electrochemical capacitors and protective coatings against corrosion [8], magnetic devices, biomaterial separation membranes [9], electronics, sensors, nanoelectronic sensor devices, biosensors, and catalysis.

Conducting polymer-incorporated metallic nanoparticles, or the so-called nanocomposites [8], exhibited synergistic unique physical and chemical characteristics based on the porous polymer and the dispersed metal [10–14]. The combination of the porous structure and high efficient electronic charge flow of the conducting polymers with the high reactive surface area presented by noble metal nanoparticles resulted in interesting electrocatalytic properties [15]. As well, the development of the composite material aims to enhance the electrocatalytic properties of the simple polymeric electrode coating [16]. Various hybrid nanocomposites were fabricated for different applications which are summarized in Table 1.

Different Routes of Formation of Polymer/Metal Nanocomposite Hybrid

There are different routes for the growing of metal nanoparticles inside the polymer matrix: chemical routes [8, 9, 20, 21], electrochemical deposition of metal

Table 1 Summary of various hybrid nanocomposites and their applications

Hybrid nanocomposites	Application	References
Pt nanoparticles' dispersed poly(3-methylthiophene)	DNA biosensor	[17]
Pd and Pt nanoclusters' modified poly(3-methylthiophene) (PMT), poly(*N*-methylpyrrole) (PMPy), and polyfuran	Sensors for simultaneous determination of catecholamine neurotransmitters and acetaminophen in the presence of uric acid and ascorbic acid	[10–13]
Gold nanoclusters' modified insulating overoxidized polypyrrole	Electrochemical biosensor for dopamine and serotonin	[18]
PEDOT/Pd composite	Electrochemical sensor for simultaneous determination of dopamine and uric acid	[19]

Table 2 Summary of the different routes of formation of polymer/metal nanocomposite hybrid

Routes of formation of polymer/metal nanocomposite	Example	References
Chemical routes for the growth of metal nanoparticles inside the polymer matrix	Chemical preparation of gold-incorporated PEDOT nanocomposite via reverse emulsion polymerization method [8] Spontaneous deposition of Au and Pt nanoparticles on polymers containing sulfur by the immersion of the polymer into the metal nanoparticle suspension (colloidal methods; citrate or borohydride reduction in the presence of citrate capping agent) [15, 17]	[8, 9, 15, 17, 20, 21]
Electrodeposition of polymer and metal nanoparticles simultaneously	PEDOT including Au nanoparticles by constant current method on ITO glass in aqueous medium [26]	[14, 24–26]
Electrodeposition of metal nanoparticles on the spin-coated polymer		[22]
Electrochemical deposition of metal nanoparticles on the electropolymerized polymer	Electrodeposited Au nanoparticles by bulk electrolysis BE method (at −400 mV for 400 S) over the electrochemically prepared PEDOT film by BE at 1400 mV for 30 S [27] Nano-Au/PPy_{ox} composite by electrochemical polymerization of pyrrole by cycling the potential from −0.35 to 0.85 V for 3 cycles. Then, Au nanoclusters were electrochemically deposited on the PPy_{ox}/GCE by cycling the potential between 0.2 and −1.0 V in $HAuCl_4$ solution for 15 cycles [18]	[7, 18, 19, 23, 27, 28]

nanoparticles on the polymer matrix that was prepared by spin coating [22] or electrochemical methods [23], and electrodeposition of polymer and metal nanoparticles simultaneously [14, 24, 25]. Summary of the different routes of formation of polymer/metal nanocomposite hybrid is given in Table 2.

Characterization of Nanometallic Particles/Polymer Composite

Surface and Chemical Characterization

Scanning electron microscope (SEM) is an electrochemical tool which gives an image for the different studied surfaces explaining their morphology in relation to electrocatalytic activity. Pd nanoparticles electrodeposited on poly(3-methylthiophene) (PMT) film-modified Pt electrode was utilized as novel electrochemical biosensor. The electrocatalytic activity of the obtained nanocomposite is affected to a great extent by the polymerization method of the polymer (bulk electrolysis BE, cyclic voltammetry CV) and the deposition method of Pd nanoparticles. Pt/PMT (BE), Pt/PMT(CV), Pt/PMT(BE)/Pd(BE), and Pt/PMT(BE)/Pd(CV) showed great difference in their electrocatalytic response which can be explained in terms of their morphology analyses (Fig. 2a–e). Pt/PMT(BE) exhibited a compact morphology with low porosity but Pt/PMT(CV) showed fluffy surface with high porosity. On the other hand, Pd nanoparticles are larger with dendrite forms at Pt/PMT(BE)/Pd(BE), while smaller Pd particles with homogenous distribution are observed at Pt/PMT(BE)/Pd(CV). In a conclusion, the electrocatalytic activity of the modified electrodes is highly affected by the size and homogeneity of the deposited nanoparticles [11].

Furthermore, the loading of the metal nanoparticles on the polymer matrix can be confirmed using energy dispersive X-ray analysis (EDX). Atta et al. constructed a novel biosensor by the electrodeposition of Pt or Pd nanoparticles into poly(3-methylthiophene) (PMT) matrix. BE technique was used to prepare PMT film at 1800 mV for 30 s. Then, metal nanoparticles were electrodeposited by double potential step (BE) method. The formed electrode can be represented as Pt/PMT(240 or 360 nm)/M, M: Pt or Pd particles. EXD analysis was performed to investigate the ratio of the loaded Pd/Pt over the polymer film corresponding to its value in the deposition solution and to confirm the immobilization of metal nanoparticles over the polymer matrix. The deposition solution contained equimolar amounts of $PdCl_2$ and $PtCl_2$. Figure 3 showed the EDX analysis explaining the atomic percentages of 47.22 and 52.78 corresponding to Pd and Pt, respectively, which is very close to their ratio in the deposition solution [11].

XRD

XRD was used to confirm the formation of polymer incorporating metal nanoparticles. Gold nanoparticles are dispersed in the PEDOT backbone that was polymerized in a linear fashion. The XRD patterns of PEDOT and Au-incorporated PEDOT nanoparticles are shown in Fig. 4. No characteristic peaks are observed in case of PEDOT, except the low angle peak at ~25° which is characteristic to the amorphous nature of the polymeric material. On the other hand, the diffraction characteristic peaks for PEDOT–Au nanocomposite appeared at 2θ 38.20°, 44.41°, 64.54°, 77.50°, and 81.68° corresponding to (111), (200), (220), (311), and (222) planes of the standard cubic phase of Au, respectively [8, 9, 28]. The broadening of XRD peaks suggests the formation of nanocrystallites. The average particle size of Au nanoparticles was ~50 nm based on Scherrer equation [8].

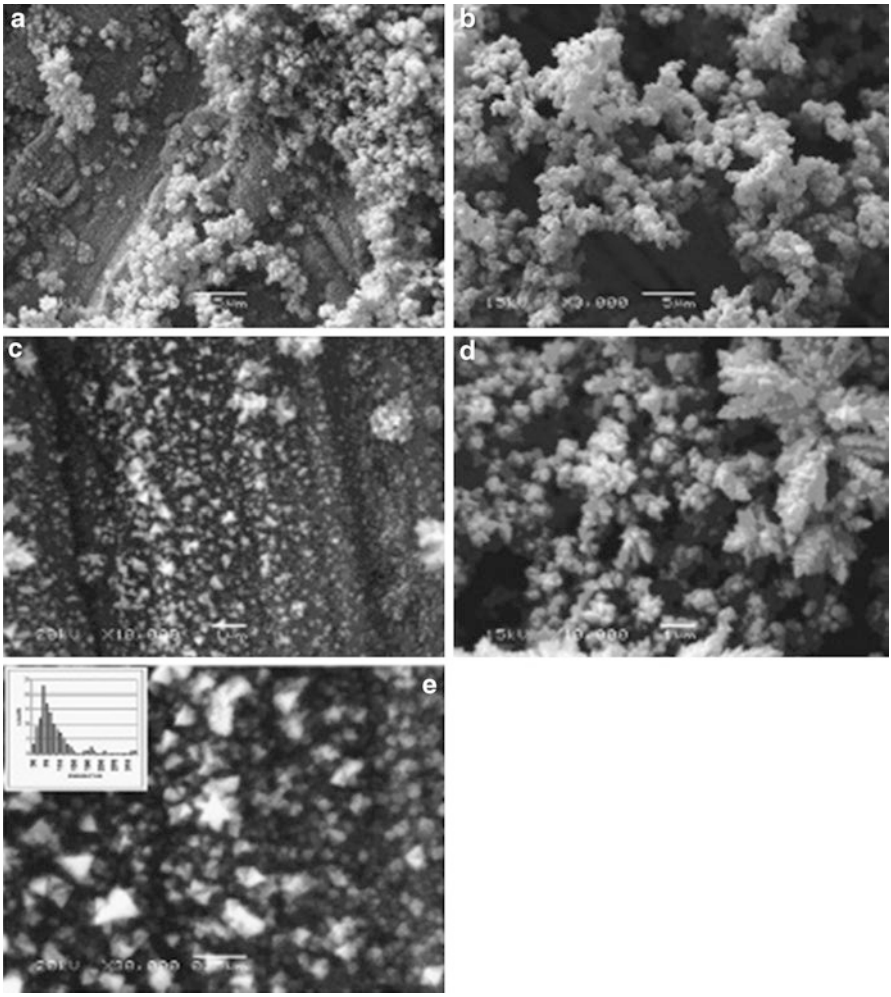

Fig. 2 Scanning electron micrographs for (**a**) Pt/PMT(BE), (**b**) Pt/PMT(CV), (**c**) Pt/PMT(BE)/Pd(BE), and (**d**, **e**) Pt/PMT(BE)/Pd(CV). *Inset*: histogram showing the Pd particle size distribution; average size is around 60 nm (Reprinted from [11], Copyright (2010), with permission from Elsevier)

AFM

Topography and properties of different surfaces can be measured using atomic force microscope. Figure 5a, b shows the AFM 3D images of Au/PEDOT and Au/PEDOT–Au_{nano} electrodes by the noncontact mode, respectively [27].

XPS

X-ray photoelectron spectra (XPS) can be used to confirm the incorporation of metal nanoparticles on the polymer film. Y. Lee prepared PEDOT/Au nanocomposite using a redox cycle system. Two strong signals of Au $4f_{5/2}$ and $4f_{7/2}$ energy levels

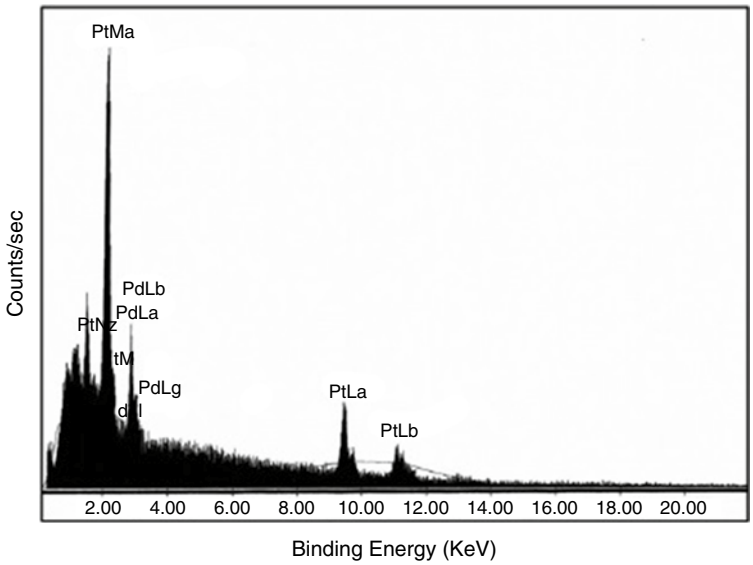

Fig. 3 Energy dispersive analysis by X-ray, EDAX, for Pt/PMT/(Pd+Pt) electrode. Pd and Pt were deposited by the double potential step method from a solution of 2.5 mM $PdCl_2$+2.5 mM $PtCl_2$/0.1 M $HClO_4$ (Reprinted from [11], Copyright (2010), with permission from Elsevier)

were centered at 84.4 and 88.0 eV, respectively, indicating the presence of metallic gold [21] (Fig. 6). Moreover, Ce Wang utilized Pt/polypyrrole (PPy) hybrid hollow microspheres as electrocatalysts for hydrogen peroxide reduction. Pt/polypyrrole was prepared by wet chemical method via Fe_3O_4 template. Figure 7 showed the XPS patterns of Pt/polypyrrole composites showing a significant Pt4f signal due to the binding energy of metallic Pt (Fig. 7a), a C1s signal due to the binding energy of C (Fig. 7b) and a N1s signal corresponding to the binding energy of N (Fig. 7c). Therefore, XPS can be used to confirm the formation of Pt/PPy hybrid hollow spheres by the wet chemical method using Fe_3O_4 template [29].

FTIR

FTIR can be used to illustrate the molecular structure of nanocomposites. FTIR spectroscopy was used to characterize the molecular structure of the Pt/PPy hybrid hollow spheres. Figure 8 investigated the characteristic bands of the Pt/PPy hybrid hollow spheres which are the pyrrole ring fundamental vibrations. The characteristic bands appeared at 1564 cm^{-1} (C=C stretching), 1456 cm^{-1} (C–C stretching), 1338 cm^{-1} (C–N stretching vibration in the ring), 1068 cm^{-1} (C–H deformation vibration), 1132 cm^{-1} (C–C breathing), 3461 cm^{-1} (N–H stretching mode), and 846 cm^{-1} (C–H out of plane vibration). The FTIR spectra of Pt/PPy hybrid hollow spheres and Fe_3O_4/PPy spheres showed no obvious difference indicating that no chemical bonds exist between Pt nanoparticles and PPy shell [29].

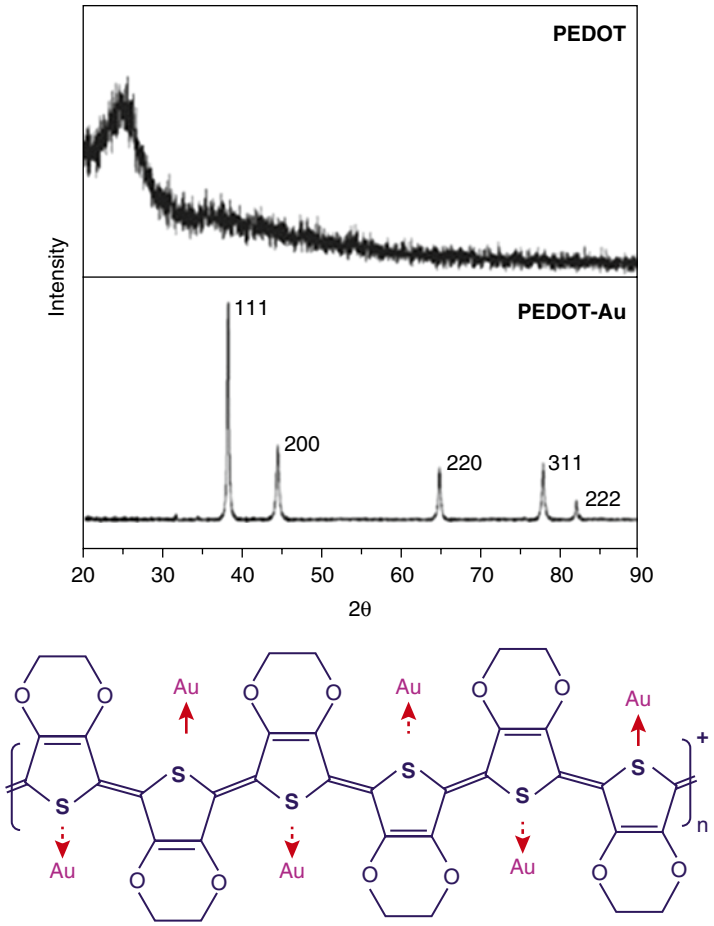

Fig. 4 XRD pattern of nanoparticles of PEDOT and Au–PEDOT nanocomposite and schematic diagram showing Au nanoparticles incorporated within the polymer backbone (Reprinted from [8], Copyright (2007), with permission from Elsevier)

On the other hand, the FTIR spectrum of the PEDOT film and monomer is shown in Fig. 9. The formation of PEDOT chains with α, á-coupling can be demonstrated by the disappearance of the strong band at 890 cm^{-1} (C–H bending mode) in the polymer spectrum compared to the monomer spectrum. Thiophene ring exhibited vibrations at 1518, 1483, and 1339 cm^{-1} due to C=C and C–C stretching modes. C–S bond vibration modes in the thiophene ring appeared at 978, 842, and 691 cm^{-1}. The stretching modes of ethylenedioxy group appeared at 1213 and 1093 cm^{-1}. The band around 920 cm^{-1} is attributed to the ethylenedioxy ring deformation mode. On the other hand, the doped state of PEDOT usually shows an absorption peak at 1722 cm^{-1}. The intensity increases in the case of Au-incorporated polymer matrix as a result of Au_{nano} doping within the polymer matrix [8].

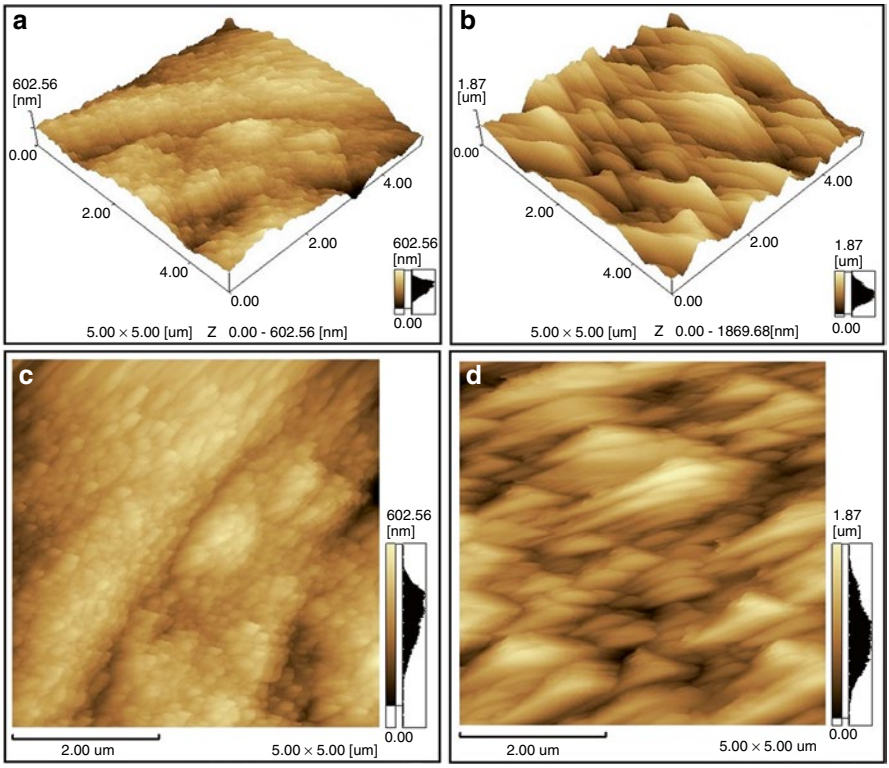

Fig. 5 3D AFM images of Au/PEDOT (**a**) and Au/PEDOT–Au_{nano} (**b**) electrodes by noncontact mode. 2D AFM images by noncontact mode of Au/PEDOT (**c**) and Au/PEDOT–Au_{nano} (**d**) electrodes (Reprinted from [27], Copyright (2012), with permission from Elsevier)

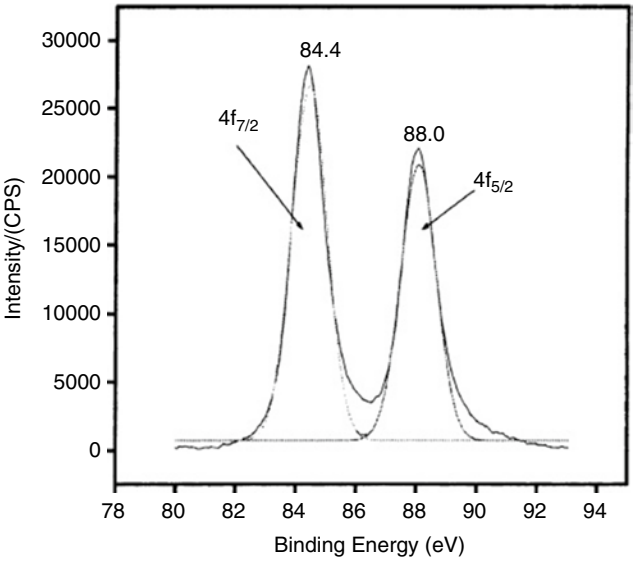

Fig. 6 XPS spectrum of PEDOT/Au composite film (Reprinted from [21], Copyright (2005), with permission from Elsevier)

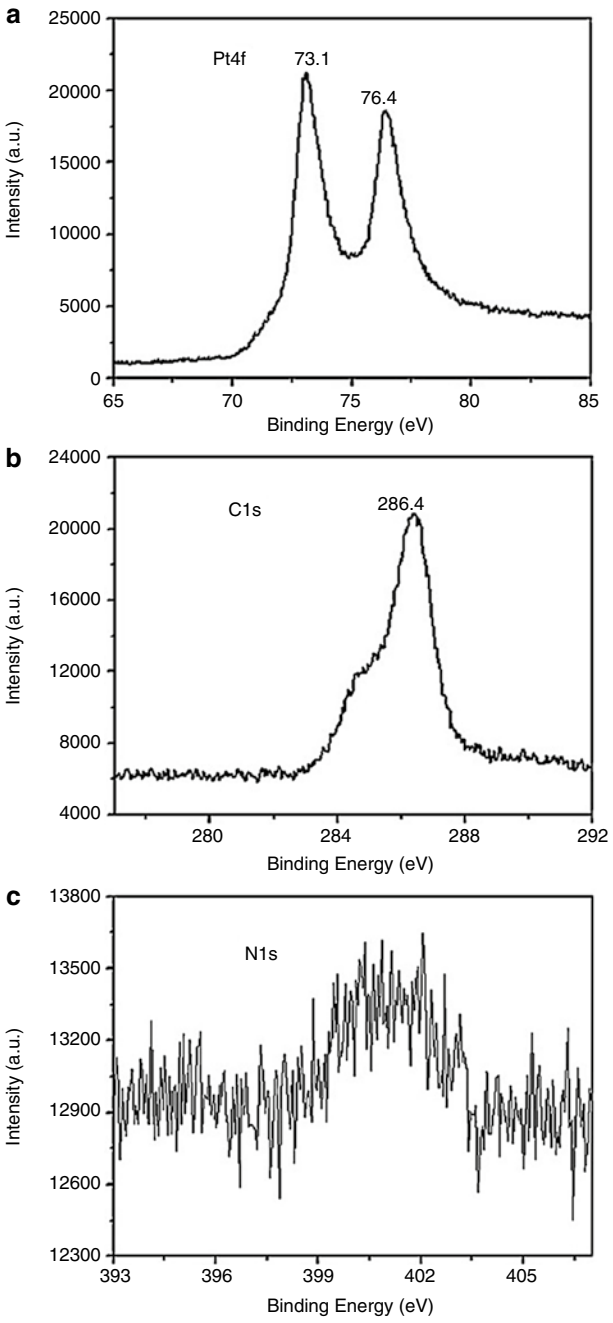

Fig. 7 XPS patterns of the Pt/PPy hybrid hollow spheres: (**a**) Pt 4f; (**b**) C 1 s; (**c**) N 1 s (Reprinted from [29], Copyright (2010), with permission from Elsevier)

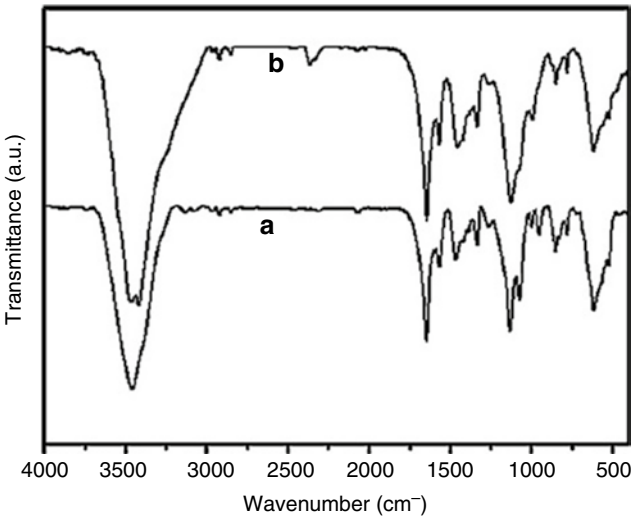

Fig. 8 FTIR images of (*a*) Fe_3O_4/PPy composites and (*b*) Pt/PPy hybrid hollow microspheres (Reprinted from [29], Copyright (2010), with permission from Elsevier)

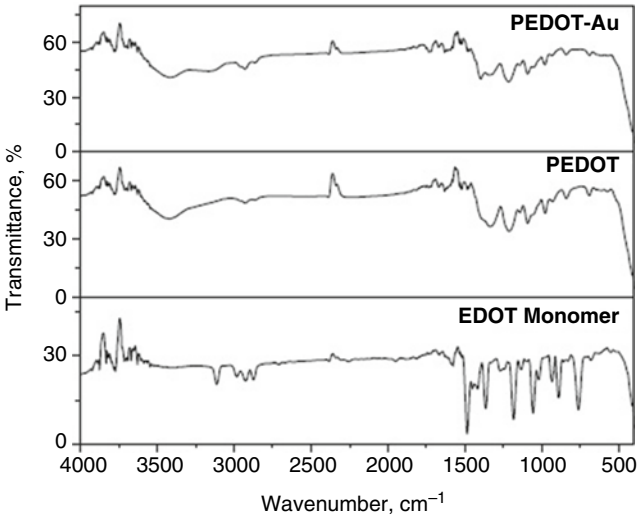

Fig. 9 FTIR spectrum of EDOT monomer, PEDOT, and Au–PEDOT nanocomposite (Reprinted from [8], Copyright (2007), with permission from Elsevier)

Sensing Applications

Polymer/metal nanocomposites have been widely utilized as sensor and biosensors. Pd nanoparticles distributed into conductive polymer matrix of poly(3-methylthiophene) (PMT), poly(*N*-methylpyrrole) (PMPy), or polyfuran (PF) film-coated Pt electrode were utilized as biosensors for neurotransmitters and

acetaminophen. Different parameters were studied because they have a great effect on the electrocatalytic activity of the resulting nanocomposite such as polymer film thickness, its polymerization method, type of deposited metal nanoparticles, metal nanoparticles deposition method, deposition voltage, and its amount. The resulting hybrid nanocomposite combined the perfect properties of the polymer matrix and metal nanoparticles. This combination resulted in dramatic enhancement in the electrocatalytic activity of the modified electrodes toward the studied compounds. In addition, the interference of ascorbic and uric acids (AA and UA, respectively) and other interferents with the studied analyte was eliminated at the surface of these modified electrodes showing perfect selectivity and anti-interference ability [10–13].

The enhanced electrocatalytic effect of Pt/PMT/Pd nanocomposites was highly affected by the method of formation of polymer film (bulk electrolysis (BE), cyclic voltammetry (CV)) (Fig. 10a). Cyclic voltammetry technique was used to test the resulting Pd-modified PMT electrodes in 5 mM hydroquinone (HQ). Pt/PMT(BE)/Pd(CV) nanocomposite exhibited higher electrocatalytic activity compared to Pt/PMT(CV)/Pd(CV) electrode as it exhibited higher oxidation current, lower oxidation potential, and smaller peak separation.

Another factor that affects the electrocatalytic activity of polymer/metal nanocomposite is the conducting polymers' doping level. After the formation of PMT polymer with BE method, the film was washed with acetonitrile and dedoped in a solution free from the monomer (0.05 M Bu_4NPF_6/CH_3CN) for 1 min at –0.2 mV. Then, Pd nanoparticles were electrodeposited using CV over the dedoped polymer film (Scheme 1). Pt/PMT(dedoped) exhibited lower current response, larger peak separation, and broader oxidation peak compared to the doped one (Fig. 10b). The inclusion (doping) and expulsion (dedoping) of the given anion resulted in reorganization of polymer chains which resulted in further conformational changes and structural differences leading to broader oxidation peaks at the dedoped films. In a conclusion, the electroactivity of the Pt/PMT and Pt/PMT/Pd electrodes toward HQ electrooxidation is greatly affected by the doping level of the PMT film [11, 12].

As well, the electrocatalytic activity of the resulting hybrid nanocomposite is highly affected by the method of deposition of Pd particles (BE and CV). The electrochemistry of bare Pt, Pt/PMT(BE), Pt/PMT(BE)/Pd(BE), and Pt/PMT(BE)/Pd(CV) electrodes toward 5 mM HQ was shown in Fig. 11. The current response was enhanced by 3.88- and 6.18-fold at Pt/PMT(BE)/Pd(BE) and Pt/PMT(BE)/Pd(CV) electrodes, respectively, compared to bare Pt. Also, the oxidation potential was shifted to less positive potential by 119 and 107 mV at the same electrodes. Pt/PMT(BE)/Pd(CV) electrode can catalyze the electrooxidation of HQ greatly due to the enhancement of peak current and the decrease in the oxidation potential. On the other hand, the effect of interference from UA on the simultaneous determination of DA and AA was investigated at Pt/PMT(BE)/Pd(CV) electrode. Three well-resolved peaks were defined at the modified electrode at −128 mV, +113 mV, and +400 mV for AA, DA, and UA, respectively. As a result of this good separation, the simultaneous determination of the three components can be achieved well at this modified electrode. Also, glucose and other interferents did not show any interference with

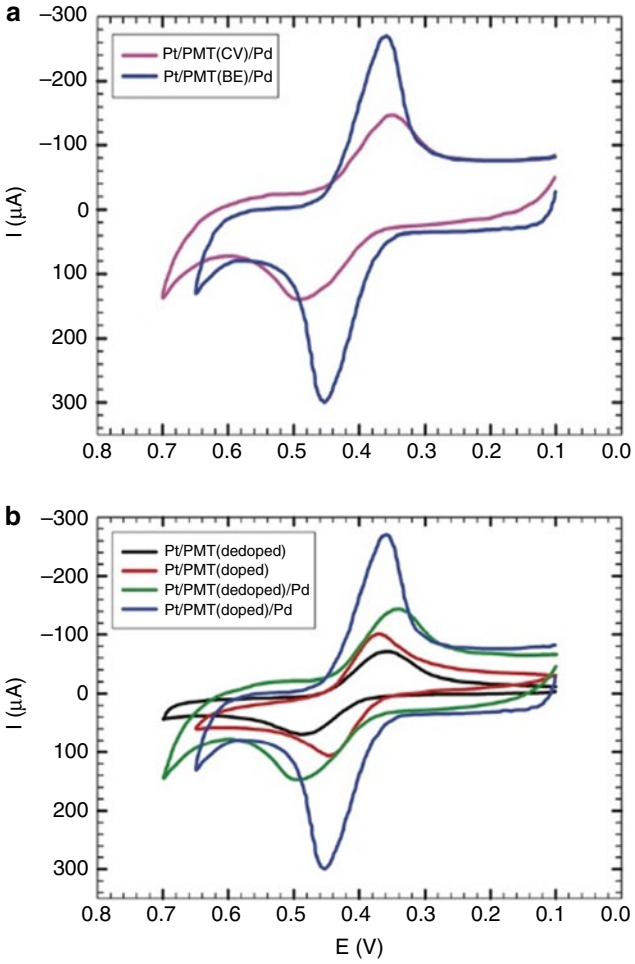

Fig. 10 Effect of the method of PMT formation (**a**) and doping level of PMT films (**b**) on the electroactivity of the produced PMT–Pd hybrid. The electrodes are tested in 5 mM HQ/0.1 M H_2SO_4 at a scan rate of 50 mV s^{-1} (Reprinted from [11], Copyright (2010), with permission from Elsevier)

the studied species [11, 12]. On the other hand, the simultaneous determination of a quaternary mixture containing AA, HQ, DA, and acetaminophen (APAP) in 0.1 mol L^{-1} H_2SO_4 was achieved at Pt/PMT(BE)/Pd (CV) electrode. Four well-defined peaks were obtained at Pt/PMT(BE)/Pd (CV) electrode: 264, 408, 504, and 656 mV for AA, HQ, DA, and APAP, respectively [12].

Randles–Sevcik equation was used to calculate the apparent diffusion coefficient D_{app} for DA at Pt/PMPy(BE), Pt/PMPy(CV), Pt/PMPy(BE)/Pd_{nano}(BE) (I), and Pt/PMPy(BE)/Pd_{nano}(CV) (II). The order of the increase of D_{app} values was Pt/PMPy(BE) ~ Pt/PMPy(CV) < Pt/PMPy(BE)/Pd_{nano} (I) < Pt/PMPy(BE)/Pd_{nano} (II).

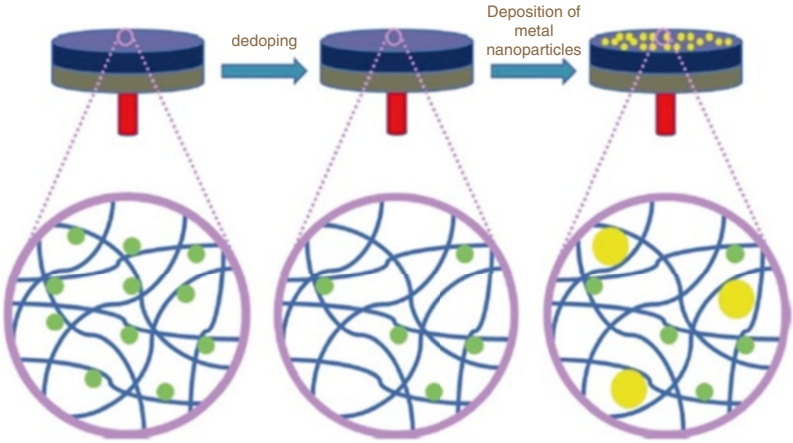

Scheme 1 Schematic diagram showing the mechanism of undoping and loading of nanoparticles into the polymer matrix (Reprinted from [11], Copyright (2010), with permission from Elsevier)

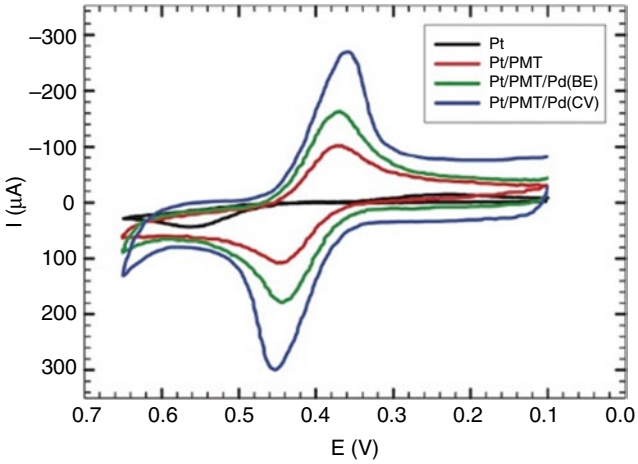

Fig. 11 Comparison between the different electrodes formed by the electrodeposition of Pd on PMT films. Cyclic voltammograms obtained by testing the electrodes in 5 mM HQ/0.1 M H_2SO_4 solution at a scan rate of 50 mV s^{-1} (Reprinted from [11], Copyright (2010), with permission from Elsevier)

The analyte diffusion increased due to the inclusion of Pd nanoparticles in the polymer matrix; the D_{app} values calculated at Pt/PMPy(BE)/Pd_{nano} (II) for some analytes are 100 times greater than that at Pt/PMPy electrodes. D_{app} values obtained at Pt/PMPy(BE)/Pd_{nano} (II) are close to those found in aqueous solution (10^{-5} cm^2 s^{-1}) because of the fast mass transfer of the analyte species from bulk solutions toward electrode surface and/or fast electron transfer process of analyte electrochemical

oxidation at the electrode surface/solution interface. In addition, the analyte redox reaction occurs at the electrode surface controlled with the molecules diffusion from the solution bulk to the electrode surface. The analyte redox reaction does not occur within the polymer/Pd_{nano} matrix. As the DA molecule reaches the Pt/PMPy/Pd_{nano} surface, it simultaneously undergoes oxidation due to the greater number of active sites on this surface. On the other hand, DA diffuses on the Pt/PMPy surface until it finds the active site for oxidation. The previous results showed that the electrodeposited Pd_{nano} has a great electrocatalytic effect on the electrochemistry of the studied species [10].

Figure 12 showed the differential pulse voltammograms (DPV) of different micromolar concentrations of DA and UA at Pt/PMPy(BE)/Pd_{nano}(II) and different millimolar concentrations of AA. The oxidation peak currents of DA, UA, and AA increased with the increase in their concentrations in the working concentration range. For AA, the linear dynamic range was 0.05–1 mM with 0.9993 correlation coefficient and 0.0056 μA/μM sensitivity. For DA, the linear dynamic range was 0.1–10 μM with 0.9995 correlation coefficient and 0.71 μA/μM sensitivity. For UA, the linear dynamic range was 0.5–20 μM with 0.9991 correlation coefficient and 0.28 μA/μM sensitivity. The potential peak separations were large enough for the individual and simultaneous determination of DA, UA, and AA. The obtained

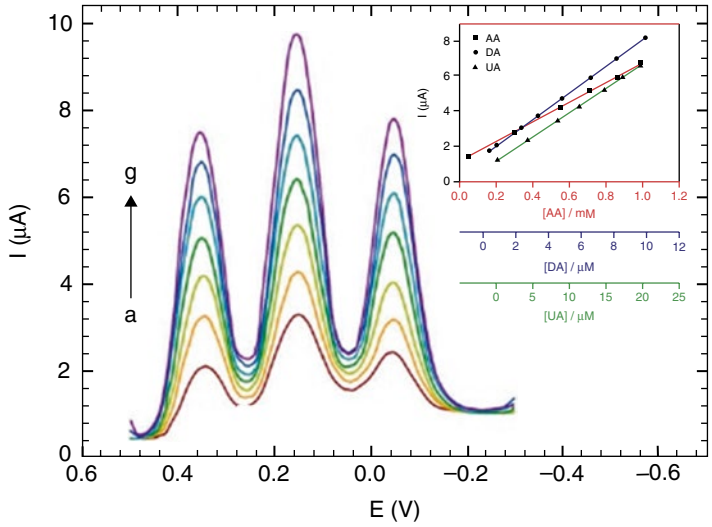

Fig. 12 Simultaneous determination of AA, DA, and UA. Differential pulse voltammograms of AA, DA, and UA were obtained at Pt/PMPy(BE)/Pd_{nano}(II) in 0.1 M PBS (pH 7.4). Concentrations of the three compounds (*a–g*): AA (0.05, 0.2, 0.34, 0.55, 0.72, 0.87, and 1.0 mM), DA (0.1, 1.7, 3.2, 4.8, 6.4, 8.0, and 10.0 μM), and UA (0.5, 5.0, 8.5, 11.5, 15.3, 18.0, and 20.0 μM). *Inset*: the peak current of AA, DA, and UA increases linearly over a concentration range typical of physiological conditions. Interestingly, the difference between peak potentials does not change with the concentration of the three species in the mixture (Reprinted from [10], Copyright (2010), with permission from Elsevier)

values of detection limit (signal/noise [S/N] = 3) at Pt/PMPy(BE)/Pd_{nano}(II) were 12 nM, 27 nM, and 7 μM for DA, UA, and AA, respectively. Also, the detection limits of DA were not affected by the absence and presence of UA and AA (14 and 12 nM, in the absence and presence of AA and UA, respectively). These results confirmed the independent oxidation processes of AA, DA, and UA and their independent simultaneous determination [10].

Furthermore, Atta et al. studied the simultaneous determination of AA, DA, and acetaminophen ACOP at bare Pt, Pt/PF(BE), and Pt/PF(BE)/Pd(CV) in 0.1 M H_2SO_4. The voltammetric signals of AA, DA, and ACOP were not resolved at bare Pt and Pt/PF(BE). On the other hand, three well-resolved voltammetric signals were resolved at Pt/PF(BE)/Pd(CV) at 246, 508, and 673 mV for AA, DA, and ACOP, respectively. The presence of AA affected the determination of the actual concentration of DA as the dopamine-*o*-quinone "DA oxidation product" reacts catalytically with AA and regenerates DA again by the reduction of dopamine-*o*-quinone. At Pt/PF(BE)/Pd(CV), AA is oxidized before DA, and large potential separation (262 mV) between AA and DA was achieved. As a result, the interference from the oxidation product of DA was minimized. In a conclusion, the synergistic presence of PF and Pd in the new composite affected greatly the simultaneous determination of AA, DA, and ACOP [13].

On the other hand, PEDOT-incorporated gold nanoparticles were prepared by J. Mathiyarasu via chemical and electrochemical routes and were utilized for DA and UA sensing in presence of excess AA. A distribution of reduced (hydrophobic) and oxidized (hydrophilic) regions was present in the PEDOT matrix. Au_{nano} has the tendency to reside within the "hydrophobic regions" of PEDOT. DA is considered one of the hydrophobic analytes; therefore, DA interacts with the hydrophobic regions. On the other hand, the hydrophilic analytes like AA interact with hydrophilic regions of PEDOT (Scheme 2) [14, 25]. Figure 13 showed the electrochemistry of DA and UA in the presence of excess of AA at Au_{nano}–PEDOT nanocomposite. Au_{nano}–PEDOT nanocomposite exhibited more efficient response toward DA and UA. The detection limit of DA/UA in the presence of 0.5 mM of AA was 2 nM. The PEDOT matrix allowed perfect peak potential separation for the studied species exhibiting excellent selectivity. The gold nanoparticles allowed the nanomolar

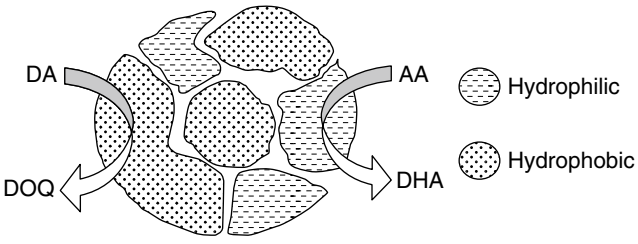

Scheme 2 Depiction of hydrophobic and hydrophilic regions on the conducting polymer film; *DOQ* dopamine-*o*-quinone, *DHA* dehydroascorbate (Reprinted from [25], Copyright (2005), with permission from Elsevier)

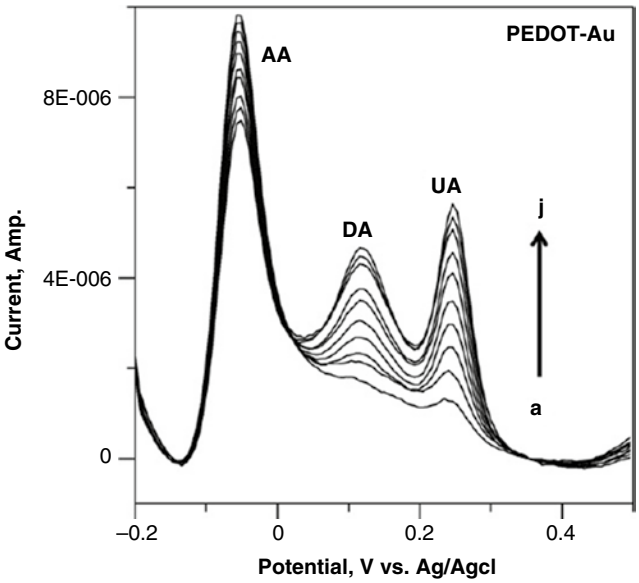

Fig. 13 Differential pulse voltammograms of Au–PEDOT-coated electrode in phosphate buffer solution (pH 7.4) containing 0.5 mM AA with different concentrations of DA and UA (*a–j* correspond to mixed solutions of 2, 4, 6, 8, 10, 12, 14, 16, 18, and 20 nM) (Reprinted from [14], Copyright (2008), with permission from Elsevier)

determination of these species exhibiting high sensitivity [14]. Therefore, Au_{nano}–PEDOT nanocomposite can detect DA and UA sensitively and selectively in the presence of AA.

Moreover, Pd/PEDOT/GCE enhanced the current response and the reversibility of DA in comparison with bare GCE and PEDOT/GCE. The DA oxidation process at the nanocomposite does not cause any fouling of the electrode surface. Also, simultaneous determination of DA and UA in the presence of AA was achieved at Pd/PEDOT/GCE. Good peak potential separations of 190 and 320 mV were achieved between DA–AA and UA–AA, respectively [19]. Moreover, poly(4-aminothiophenol) (PAT)–Au_{nano} was utilized for the simultaneous determination of AA and DA showing two well-resolved anodic peaks at 75 and 400 mV for AA and DA, respectively. The nanocomposite exhibited good selectivity and high sensitivity without fouling by AA or DA oxidation products. Also, PAT–Au_{nano} was utilized for the real determination of DA in human blood serum. No interference from AA, UA, albumin, and glucose was observed (Table 3) showing an applicable selective and sensitive DA sensor in real samples. In addition, long-term stability was observed for DA electrochemical response (>15 days) [28].

On the other hand, Nano-Au/PPy_{ox} composite-coated GCE was developed by Xiangqin Lin as an electrochemical biosensor for DA and serotonin 5-HT,

Table 3 Determination of DA in human blood serum ($n=5$) (Reprinted from [28], Copyright (2007), with permission from Elsevier)

Samples	Added (μmol L^{-1})	Found (μmol L^{-1})	Recovery (%)	R.S.D %
1	0.3	0.32	101	2.3
2	0.6	0.57	98	2.4
3	0.9	0.89	96	2.0

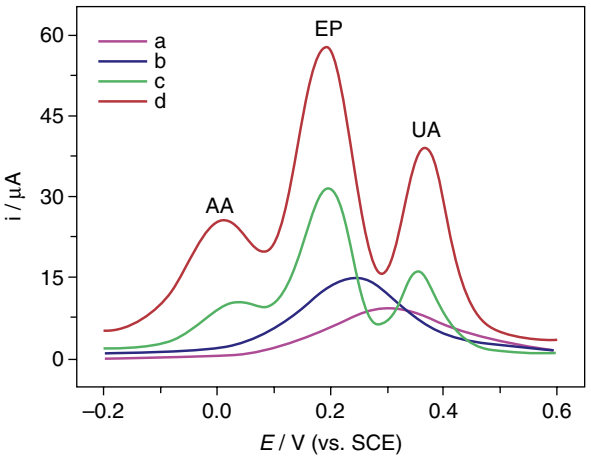

Fig. 14 DPVs of 1.0×10^{-5} M EP and 2.5×10^{-5} M UA in pH 7.0 PBS containing 5.0×10^{-3} M AA at bare GCE (*a*), nano-Au/GCE (*b*), PPyox/GCE (*c*), and nano-Au/PPyox/GCE (*d*) (Reprinted from [30], Copyright (2007), with permission from Elsevier)

exhibiting stable and sensitive current responses toward their oxidation. Gold nanoclusters were electrochemically deposited on ultrathin overoxidized polypyrrole (PPy_{ox}) film. There is a remarkable enhancement in the DA and 5-HT oxidation response current and a lowering of overpotential due to the synergic effect of the utilized composite. An enlarged template for the growth of Au nanoclusters was provided by the nanoporous PPy_{ox} film on the GCE, resulting in an array of nano-Au electrodes, enlargement in the effective surface area, and enhancement in the electronic conductivity of the composite. Therefore, the sandwiched Au nanoclusters can facilitate the mass and electronic transportation rates of the reactions of DA and 5-HT. The overlapping anodic peaks of 5-HT, DA, and AA (1000-fold) were simultaneously resolved at the modified electrode into three well-defined voltammetric peaks at 370, 200, and 10 mV (vs. SCE), respectively. The oxidation process of DA and 5-HT was adsorption-controlled as investigated by scan rate effect. A linear response was obtained in the range of 7.0×10^{-9} to 2.2×10^{-6} M with a detection limit of 1.0×10^{-9} M for 5-HT and in the range of 7.5×10^{-8} to 2.0×10^{-5} M with a detection limit of 1.5×10^{-8} M for DA (s/n=3), respectively [18]. Moreover, this novel biosensor (nano-Au/PPy_{ox}/GCE) exhibited strong catalytic activity toward the oxidation of epinephrine (EP), UA, and AA with three well-defined peaks with a large anodic peak difference. Figure 14 shows the DPV curves of 1.0×10^{-5} M EP and 2.5×10^{-5} M UA solution containing 5.0×10^{-3} M AA at

different electrodes. A broad small anodic peak at 0.31 V was obtained at bare GC electrode (curve a). Moreover, only one broad anodic peak at 0.25 V was obtained at nano-Au/GCE (curve b). However, three well-defined peaks were resolved at both PPy_{ox}/GCE (curve c) and nano-Au/PPy_{ox}/GCE (curve d). An enhancement in the oxidation currents of EP, AA, and UA was obtained at nano-Au/PPy_{ox}/GCE than that at PPy_{ox}/GCE, indicating that the nanocomposite has a strongly electrocatalytic activity toward EP, UA, and AA oxidation. In addition, the sensor exhibited excellent sensitivity, selectivity, and stability and has been applied for determination of EP in epinephrine hydrochloride injection and UA in urine samples with satisfactory results [30].

Moreover, a hybrid nanocomposite of PEDOT and Au-NPs is fabricated electrochemically onto a screen-printed carbon electrode (SPCE). SPCE/PEDOT/Au-NPs-modified electrode exhibited great catalytic activity for the oxidation of cysteine in various pH buffer solutions (pH 2.0–8.0). The selectivity of the method is demonstrated by the separation of the oxidation peaks at up to 240 mV for cysteine and glutathione in pH 6.0 buffer solutions. Flow-injection amperometry is performed for 0.5–200 μM of cysteine in pH 4.0 buffer solutions, and a linear calibration plot with a slope of 0.115 μA/μM is obtained with detection limit (S/N = 3) 0.05 μM. Additionally, the proposed methods obtain satisfactory results in the detection of cysteine-containing medicine samples [23].

Moreover, Pt/polypyrrole (PPy) hybrid hollow microspheres were utilized by Ce Wang as enzymeless electroactive H_2O_2 biosensor. At bare GCE, no H_2O_2 reduction peak was obtained, but a H_2O_2 reduction peak appeared at − 100 mV at the proposed sensor (Fig. 15) because of the high electrocatalytic activity of the ultrahigh-density Pt nanoparticles with the mean diameters of around 4.1 nm deposited on PPy shell. The proposed composite showed some advantages such as fast response of less than 2 s with linear range of 1.0–8.0 mM, sensitivity of 80.4 mA M^{-1} cm^{-2}, and a relatively low detection limit of 1.2 μM (S/N = 3) [29].

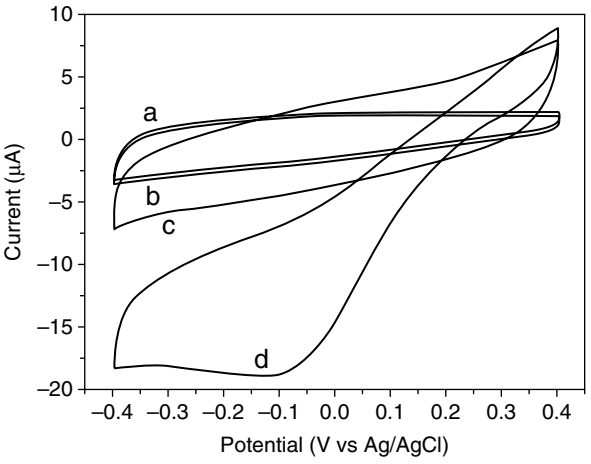

Fig. 15 CVs of H_2O_2 reduction at the bare GCE (*a* and *b*) and GCE modified by Pt/PPy hybrid microspheres (*c* and *d*) in a 0.1 M PBS in the absence (*a* and *c*) and presence of 1.0 mM H_2O_2 (*b* and *d*). The scan rate is 100 mV/s (Reprinted from [29], Copyright (2010), with permission from Elsevier)

Self-Assembled Monolayer of Surfactant on Polymers and Hybrid Nanostructures

Surfactants and Self-Assembly in Solution

Surfactants, surface active agents, are chemical compounds that have the ability to affect the interfacial relationship between two dissimilar substances such as oil and water.

Surfactants have the ability to reduce the free energy of the system by reducing the contact between the hydrophobic group and the aqueous surrounding. Surfactants are considered as amphiphilic molecules which have a hydrophilic polar head on one side and a long hydrophobic nonpolar tail on the other. They have wide potential applications in electrochemistry [31, 32]. The polar head group is characteristic with the presence of heteroatoms like N, P, S, or O. These heteroatoms are present in functional groups like alcohol, thiol, ether, ester, acid, sulfate, sulfonate, phosphate, amine, amide, etc. A hydrocarbon chain of alkyl or alkylbenzene type represented the nonpolar tail group. The unique solution and interfacial characteristics of the surfactant that resulted in enhanced electrode/solution interface property are attributed to the polar–nonpolar duality nature of the surfactants [33]. Moreover, surfactants can reduce oil–water contact by the accumulation at various interfaces or the formation of different self-assembled structures in the solution. Thus, the hydrophobic domains of surfactant molecules can associate to form various structures achieving segregation of the hydrophobic parts from water [34, 35]. Formation of a specific self-assembled structure in solution depends on the type of surfactant (the size of the hydrophobic tail group, the nature, and size of the polar head group) and the solution conditions (temperature, salt concentration, pH, etc.).

Micelles in Aqueous Medium

At low concentration surfactants form true solutions where they are dispersed as individual molecules or ions and do not associate themselves to form micelles. With increasing the concentration, spontaneous self-association in solution takes place and the srufactant molecules form micelles due to the split personality structure nature of such amphiphilic substances leads their spontaneous self-association in solution resulting in the formation of micelles [35, 36]. Aggregates of long-chain surfactant molecules or ions which are formed spontaneously in their solution at definite concentration are known as micelles which possess regions of hydrophilic and hydrophobic character. This concentration was found to be dependent on the size of the hydrophobic moiety, the nature of polar head group, the nature of counter ions (for charged surfactants), the salt concentration, pH, temperature, and presence of co-solutes. In water, the charged polar head groups are oriented toward the water, and the hydrocarbon chains are oriented

away from the water to face the interior of the micelles. Micelles are characterized by aggregation number (N) and critical micelle concentration (CMC). N is the number of molecules or monomers in the micelle determining the size and geometry of the micelle, and it ranges between 10 and 100 in aqueous solution [36]. The CMC of the amphiphile can be defined as the narrow concentration range at which the micelles first become detectable. Also, it can be defined as the concentration at which an abrupt change in physical properties like surface tension and conductivity takes place [34, 36]. Each surfactant has a characteristic CMC value where dynamic aggregates are formed. The CMC values for most surfactants are in the range of 10^{-4} to 10^{-2} mol L^{-1} [36].

Surfactants Self-Assembly at Solid/Liquid Interface

The formation of micelles in solution starts to occur upon reaching the CMC [35, 36]. At concentration less than the CMC, the cooperative hydrophobic forces are not sufficient to form micelles or any self-assembled structures in solution. As a result, surfactant molecules or ions pass out into the surface layer at the interface of the surfactant with the other phases (we will focus on solid–liquid interface), thus reducing the oil–water contact and hence lowering the free energy of the system [35]. Soon, the surface layer becomes saturated and with further increase in the surfactant concentration, the system expels the hydrophobic chains from the water into the liquid "pseudo phase" – a micelle. The adsorption of surfactants at solid substrate not only occurs before CMC but also occurs above CMC [37–41]. The adsorbed surfactant films on the surface of solid substrates exhibited different molecular structures in the form of monolayer [42–46], bilayer [47–49], multilayer (especially at extreme potentials of opposite sign for that of surfactant head group) [50–53], and surface micelles or hemimicelle (full sphere, full cylinder, or half cylinder) [54–57].

The formation of specific self-assembled structure on the solid substrate surface depends on the hydrophobicity and morphology of the substrate [58–60], the nature of the electrolyte and counter ions [61, 62], the applied potential and the charge of the substrate [63–67], the surfactant concentration [68–73], the structure and type of surfactant, and the pH of the solution from which adsorption occurs. Typical surfactant aggregate structures are shown in Scheme 3 [33, 74].

Modes of Surface Modification by Surfactants

Two important modes of modification of the electrode surface by surfactants:

1. **Surface modification**, in which spontaneous adsorption or self-assembly of surfactants occurs on the electrode surface
2. **Bulk modification**, in which surfactants (modifiers) are mixed intimately with the electrode material such as carbon paste

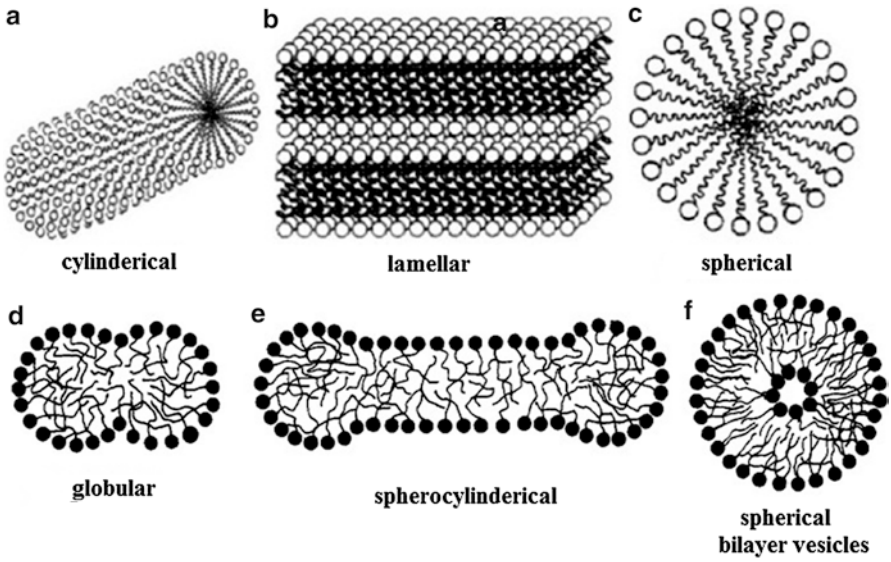

Scheme 3 Typical surfactant aggregates: (**a**) cylindrical, (**b**) lamellar, (**c**) spherical, (**d**) globular, (**e**) spherocylindrical micelles, and (**f**) spherical bilayer vesicles (Reprinted from [33, 74], Copyright (1991, 2011), with permission from Elsevier)

Surface Modification by Surfactants

Amphiphilic compounds can be used to control the electrochemistry at the modified electrode surface [75]. The adsorption of these amphiphilic compounds on the electrode surface can be achieved via different approaches [76–78]. One approach is based on the physico-chemisorption of highly ordered self-assembled monolayers (SAMs) [79]. Different self-assembled structures of surfactants were formed through the spontaneous physisorption of surfactant molecules at the electrode surface. This was achieved via the exposure of a clean electrode surface to a dilute solution of surfactants either by dipping or by the application of a drop of solution followed by spinning to evaporate the solvent (spin coating).

Effect of the Surfactants on the Electrochemical Kinetics of the Electrode Reaction

Dimensions, polarities, and molecular structures of surfactant aggregates on the electrode and the position of the electroactive species within them must be known to predict the effect of surfactants on the electrochemical kinetics of the electrode reaction [80]. Moreover, to observe the influences of the adsorbed surfactant films on the discharge of electroactive solutes on the electrode surface, it is necessary to investigate the adsorption of surfactants from aqueous solution onto the electrode surface. The most important influences of the adsorbed surfactant films on the electron transfer rates include (1) blocking by surfactants and (2) electrostatic interactions between electroactive solutes and the adsorbed surfactant films [80, 81].

The surfactant films may physically block the partial or full access of the electroactive species to the electrode surface inhibiting the electron transfer process [81]. The unfavorable entrance of hydrophilic species through the hydrophobic region of the adsorbed surfactant film or the coulombic repulsion between the charged head group of the surfactant and similar charged electroactive species was the origin of this blocking effect [82, 83]. As a result, the adsorbed surfactant film acts as a barrier between the electrode surface and the electroactive species.

On the other hand, mild kinetic enhancement for the electrode reaction may be observed due to the adsorbed surfactant film on the electrode. This enhancement depends on the preconcentration process (the accumulation of the electroactive species through or into the adsorbed surfactant film). The coulombic attraction forces as well as the hydrophobic interactions between the electroactive species and the adsorbed surfactant layers are the main driving forces for the preconcentration process [82–84]. Moreover, incorporation of electroactive species within the adsorbed surfactant films will introduce different distances between the electroactive species and the electrode surface. Thus, the rate of the electron transfer will decrease with increasing the distance between the electroactive species and the electrode surface within the adsorbed surfactant film [85–87]. This is in accordance with the electron transfer theory [88], which predicts the exponential decrease of the electron transfer rate with increasing the distance between the electroactive species and the electrode surface.

When electroactive species presents in micellar system, it may bind to the micelles present in the aqueous medium or partitioned between micelles and aqueous media [89]. Electroactive ions which are oppositely charged to the ionic micelles can bind at the micelle–water interface, whereas nonpolar electroactive species can bind in hydrophobic regions of the micelles just below this interface [90]. Electroactive species solubilized in micelles or bonded to micelles can undergo electron transfer reactions in which the current is controlled by diffusional mass transport of micelles containing the electroactive species.

Surfactant Adsorption

Surfactants have a specific amphiphilic structure which enables them to be adsorbed at the surface/interface in an oriented form [91, 92]. The adsorption of the surfactant involves the transfer of the surfactant molecules from the solution bulk to the electrode/solution interface. This adsorption process of surfactant at the solid/liquid interface plays a crucial role in many applications. There are various mechanisms by which the surfactant molecules can be adsorbed onto the solid substrates from aqueous solutions. The adsorption involves single ions rather than micelles [92].

(I) **Ion exchange** takes place through the substitution of counterions adsorbed onto the substrate from the solution by surfactant ions with similar charges.
(II) **Ion pairing** takes place through adsorption of surfactant ions from solution onto sites which are oppositely charged and unoccupied by counterions.
(III) **Hydrophobic bonding** takes place through the electrostatic attraction between a hydrophobic group of adsorbed molecule and a molecule present in the solution.

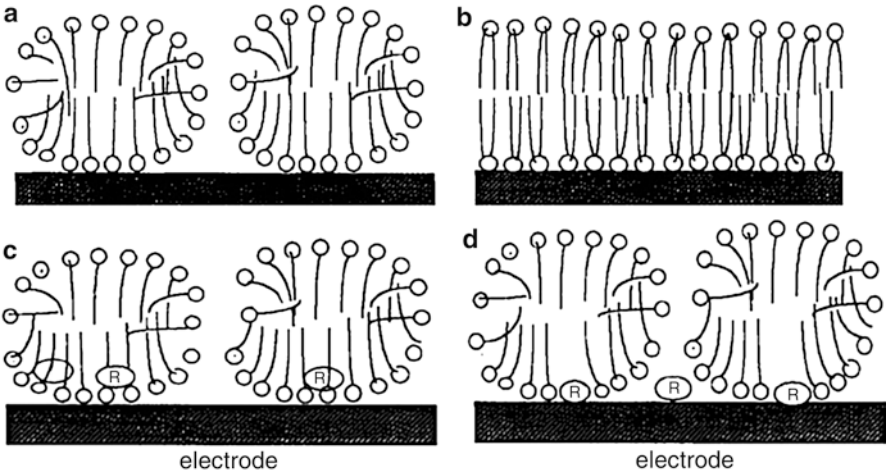

Scheme 4 Conceptual drawings of interfacial region on hydrophilic electrode in micellar solutions: (**a**) side view of surface micelles or cylinders, (**b**) side view of a bilayer, (**c**) position of reactants R which are dissolved in the surface aggregates, (**d**) position of reactants R which are specifically adsorbed to the electrode (Reprinted from [80], Copyright (1997), with permission from Elsevier)

(IV) **Adsorption by polarization of π electrons** takes place through the attraction between the electron-rich aromatic nuclei of the adsorbate "surfactant" and the positive sites on the solid adsorbent.

(V) **Adsorption by dispersion forces** takes place through the adsorption by London van der Waals force between adsorbate "surfactant" and solid adsorbent [92].

Electron Transfer Modes in Micellar Solutions

Electron transfer kinetics of electrode reaction process can be controlled by the surfactant aggregates on the electrode surface or inside the solution. Aggregates in the form of bilayers, cylinders, or surface micelles have the tendency to be adsorbed onto the electrode surface in solutions with surfactant concentration above the CMC. On hydrophilic electrodes, head-down orientations of surfactants are preferred (Scheme 4a, b) [80].

We will start by talking about the mechanism of discharge of electroactive species binding to the adsorbed dynamic surfactant film. The electron transfer process will take place when the electroactive species approaches to the vicinity of the electrode surface. Two main possibilities allow the charge transfer; the first is the displacement of the adsorbed surfactant by the reactant, thus, the reactant approaches the electrode closely (Scheme 4c), and the second is the approach of the reactant to the electrode surface within one head group diameters of adsorbed surfactant moieties (Scheme 4d). Different possibilities have been suggested for the molecular interpretation of electron transfer between a micelle-solubilized electroactive species and the electrode.

One possibility is the dissociation of solute bound to the micelle followed by its entry into the adsorbed surfactant film, then its orientation near the surface, and finally electron transfer occurs. The entry into the films and orientation are expected to occur on a millisecond time scale. Another possibility is the joining of the micelle in solution with the aggregates on the electrode surface, bringing the reactant close enough to the electrode for electron transfer [80].

The Role of Surfactants in Electrochemistry

The importance of surfactants to electrochemistry is based on the following points [93]:

(a) Surfactants in aqueous solution will affect the double layer structure, the redox potential, the charge transfer, and the diffusion coefficient of the electrode processes [91, 93].
(b) Surfactants can stabilize radicals or intermediate reaction products.
(c) Surfactants can easily dissolve hydrophobic substances.

Surfactants can endow the electrode/solution interface with different electrical properties and change the electrochemical process. For example, the adsorption of ionic surfactants can form charged surfactant layers on the electrode surface, which have a strong accumulation capacity toward the oppositely charged analytes and an electrostatic repulsion ability toward the same charged analytes. Similarly, surfactants can form loose hydrophobic layers on the electrode surface by their hydrophobic tails exhibiting a strong accumulation capacity toward hydrophobic analytes. Moreover, the formation of surfactant layers on the electrode surfaces can also avoid the direct contact of the analyte with the electrode surface enhancing the antifouling capacity of the electrodes [94, 95]. On the other hand, surfactants play a very important role in electrode reactions, not only in solubilizing organic compounds but also by providing specific orientation of the molecules at the electrode interface. Surfactants are effective excipients in many drug formulations via improving dissolution rate and increasing drug solubility. The ability of surfactants to reduce interfacial tension and contact angle between solid particles and aqueous media leads to improving the drug wettability and increasing the surface availability for the drug dissolution [96]. Accordingly, surfactants were found to have several applications in electrochemistry, polarography, corrosion, batteries, fuel cells, electrometallurgy, electroorganic chemistry, photoelectrochemistry, electrocatalysis, and electroanalysis [36]. Surfactants are very effective to be used in the electroanalysis of organic compounds, biologically important compounds, drugs, some important inorganic ions, and metals [97–99]. Moreover, micelles have also been employed as selective masking agents to improve selectivity and sensitivity of electrochemical analysis [100].

Sensor Applications of Surfactant SAM on Polymers

A promising biosensor based on poly(3,4-ethylenedioxythiophene)-modified Pt electrode (Pt/PEDOT) was constructed for DA determination in the presence of SDS. There are electrostatic interactions between the positively charged DA and the

negatively charged SDS which resulted in enhanced accumulation of protonated DA at the polymeric electrode surface, improved electrochemical response of DA, and increased current response by one and a half folds. Surfactant aggregates can be formed on the electrode surface in the form of bilayers, cylinders, or surface micelles (at higher SDS concentration), and these aggregates can explain the enhanced current response. The process of electron transfer starts when the electroactive analytes come close to the vicinity of electrode surface. The charge transfer mediation is attributed to the space of one to two head groups of adsorbed surfactant moieties extended from the surface of the electrode. On the other hand, ion pair of the protonated DA and the charged surfactant may be formed and adhered on the electrode surface via the hydrophobic parts in both sides [32]. On the other hand, three well-resolved oxidation peaks for DA, AA, and UA were defined at PEDOT/Pt in the presence of SDS. By the addition of SDS, the peak current signal of DA increases, and the peak current signals of AA and UA disappear. These observations are attributed to the electrostatic attractions between the negatively charged surfactant film and the positively charged DA which enables DA to reach the electrode surface faster. In the case of AA and UA, there are electrostatic repulsion between the anionic surfactant and the negatively charged species resulting in slower electron transfer kinetics (Scheme 5) [32].

The morphology of PEDOT matrix in the absence and presence of SDS showed a great difference (Fig. 16). In the absence of SDS, PEDOT exhibited the globular shape, and the surface appeared to be rough because of Pt substrate (Fig. 16a). In the presence of SDS, the PEDOT matrix becomes spongy and cotton-like because of the anionic tails of the surfactant (Fig. 16b). SDS aggregates have the ability to accumulate over the polymer surface and affect greatly the film conductivity [32].

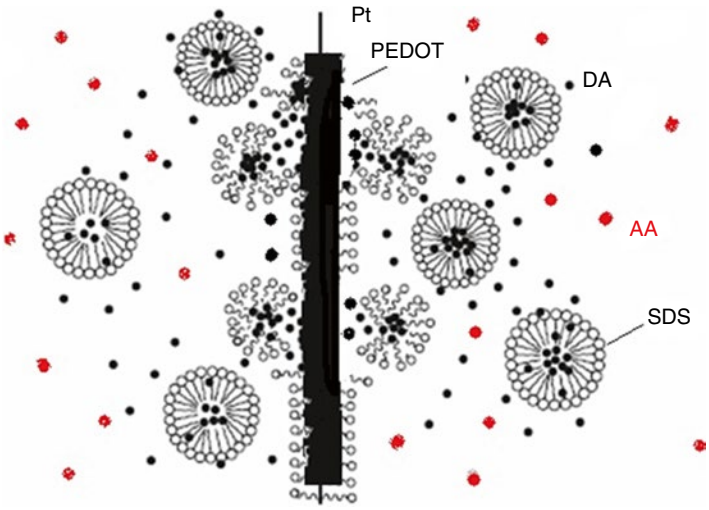

Scheme 5 Electrostatic interaction between DA cation and the PEDOT in the presence of SDS and AA (Reprinted from (Reprinted from [32], Copyright (2011), with permission from Elsevier)

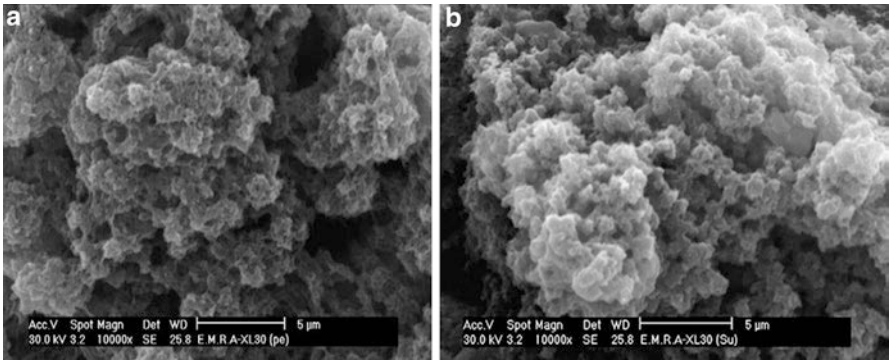

Fig. 16 SEM image of the PEDOT layers deposited on Pt wire from 0.01 mol L^{-1} EDOT in 0.1 mol L^{-1} $LiClO_4$ in acetonitrile (10 cycles) (magnification 10,000×, 30 kV), (**a**) in the absence of SDS, (**b**) in the presence of 150 µL 0.1 mol L^{-1} SDS (Reprinted from [32], Copyright (2011), with permission from Elsevier)

Furthermore, PEDOT/Pt in the presence of SDS was utilized for the determination of catecholamine compounds, namely, epinephrine, L-norepinephrine, and L-DOPA, as well as serotonin (ST). The electrochemical data for the oxidation of catecholamines, serotonin, tryptophan, acetaminophen, and some interfering compounds such as UA and AA were collected from the cyclic voltammograms at PEDOT/Pt electrode in the absence and presence of 150 µL SDS. For cationic catecholamines, an increase in the anodic and cathodic peak current values was observed upon the addition of SDS due to the electrostatic interaction between the anionic surfactant film adsorbed on the electrode and the cationic catecholamine. For anionic compounds, the oxidation current response decreases in the presence of SDS. Tryptophan, AA, and UA, which are in the anionic form at pH = 7.4, establish an electrostatic repulsion with anionic surfactant SDS resulting in a large decrease in the peak current value in micellar medium. L-DOPA and ACOP are neutral species at physiological pH (pH = 7.4), thus SDS would not affect the kinetic of these compounds. The adsorption of the surfactant molecules onto the surface of the electrode resulted in changing the oxidation current values for positively and negatively charged species, altering the electrode overpotential and affecting the kinetics of the electron transfer. Also, the micellar aggregates may influence the mass transport of the electroactive analytes toward the electrode surface [101].

On the other hand, the electrochemical response of ST in the presence of UA, AA, and glucose was investigated. The presence of more than 1000-fold excess of AA and 100-fold excess of glucose did not interfere with the response of ST. The presence of SDS in the medium plays a key role in the electrostatic attraction of ST toward the polymeric surface and causes repulsion toward the interfering species. Furthermore, both DA and ST coexist in a biological system, and they affect each other in their respective releasing. So, it was interesting to study the interaction of both compounds with SDS (Fig. 17). At PEDOT/Pt electrode, DA and ST yielded two well-defined oxidation peaks at 0.20 and 0.35 V, respectively. The current

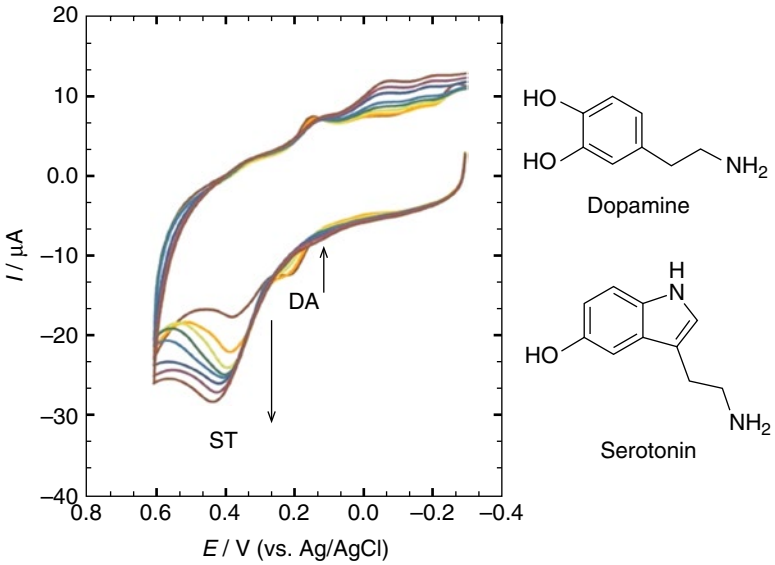

Fig. 17 Cyclic voltammograms of equimolar solution 0.5 mmol l^{-1} of both DA and ST in B-R (0.1 mol l^{-1}), scan rate 50 mV s^{-1} at PEDOT/Pt electrode pH 7.4 with successive additions of 10 μl 0.1 mol l^{-1} SDS (0–150 μl) (Reprinted from [101], Copyright (2011), with permission from Elsevier)

response of ST increased, while DA response decreased with successive additions of 150 μL SDS in 0.1 mol L^{-1} B-R pH = 7.4. This is due to the competitive interaction of DA and ST with the PEDOT/Pt film that is more pronounced in the case of ST. This is due to the large conjugated structure of ST which has the possibility to intercalate into the interior of PEDOT/Pt film. Another reason is the presence of -NH_2 and -NH groups in ST which increases the positive charge density on ST enhancing its interaction with the anionic surfactant SDS, thus facilitating its diffusion to the polymeric film [101].

Interaction of anionic SDS with ST and DA in aqueous B-R buffer solutions was followed by UV–Vis spectroscopy. Figure 18a, b shows the effect of successive additions of SDS on the absorption spectrum of each of ST and DA. The anionic SDS showed no absorption background. A band is identified at 274 nm, and a shoulder is present at 296 nm for ST due to the different possible sites of protonation in the case of indole nucleus having various constituent groups.

It was assumed that protonation on nitrogen always occurs first and then takes place in other places (Fig. 18a). The absorbance of these bands decreased from 1.31 to 0.95 with five SDS additions. On the other hand, a sharp band was formed at 279 nm for DA (Fig. 18b); its absorbance decreased from 1.27 to 0.97 with five SDS additions. The anionic character of SDS favors columbic attraction forces with the compounds and leads to the formation of aggregates in the solution phase. The aggregation in aromatic systems could be attributed to the formation of larger units (possibly due to the formation of longer repeat unit chains). This "oligomerization"

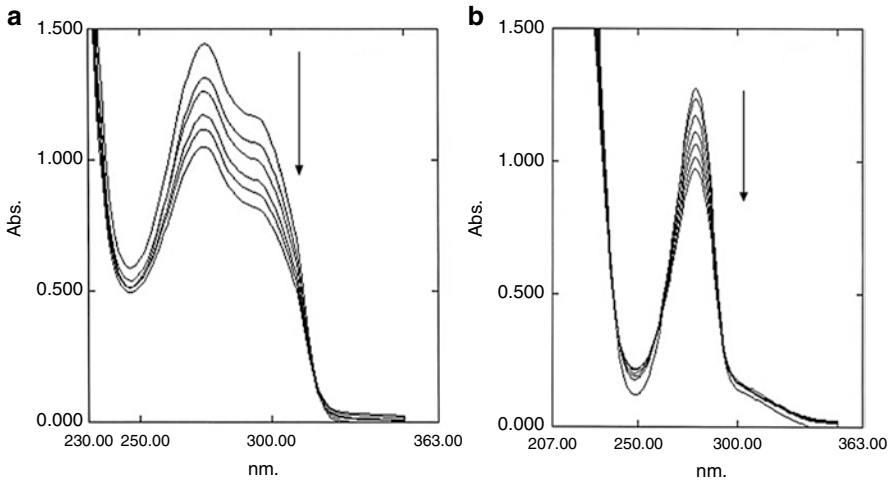

Fig. 18 Absorption spectra of five successive aliquots of 0.2 ml of 0.01 mol l^{-1} SDS added to 4.0 ml of (**a**) 2.5×10^{-4} mol l^{-1} serotonin, (**b**) 5×10^{-4} mol l^{-1} for DA (Reprinted from [101], Copyright (2011), with permission from Elsevier)

was due to the London–Margenau attractive forces between the π-electrons that are counterbalanced by the columbic and Lennard-Jones repulsive forces. This should be accompanied with a blue shift or a red shift in the corresponding spectra that was not observed in the present case for ST and DA. Thus, the charge interaction of the compound with SDS is the main contribution to the association that resulted in the decrease in the absorption spectra. Also, it was noticed from the results that the decrease in absorbance in the case of ST was larger than in the case of DA showing that there is more charge interaction of ST with SDS than in the case of DA. So, the spectrophotometry data are in good agreement with what we obtained from the voltammetry experiments [101].

On the other hand, drug analysis is an important branch of chemistry which plays an important role in drug quality control. Therefore, the development of sensitive, simple, rapid, and reliable method for the determination of active ingredient is very important [102]. Surfactants have proven effective to be used in different occasions for the electroanalysis of drugs [97–99]. Improvement of drug analysis using surfactants was found to be concentrated in two important points:

1. The ability of surfactant systems to dissolve hydrophobic (insoluble) drugs
2. The preferential accumulation of drug molecules on the electrode surface via electrostatic and hydrophobic interactions [103–108]

Atta et al. employed PEDOT/Pt for morphine (MO) determination in the presence of SDS. MO is used as a relief from severe pain. The anionic surfactant SDS facilitates the arrival of MO molecules to the electrode surface faster, improves its

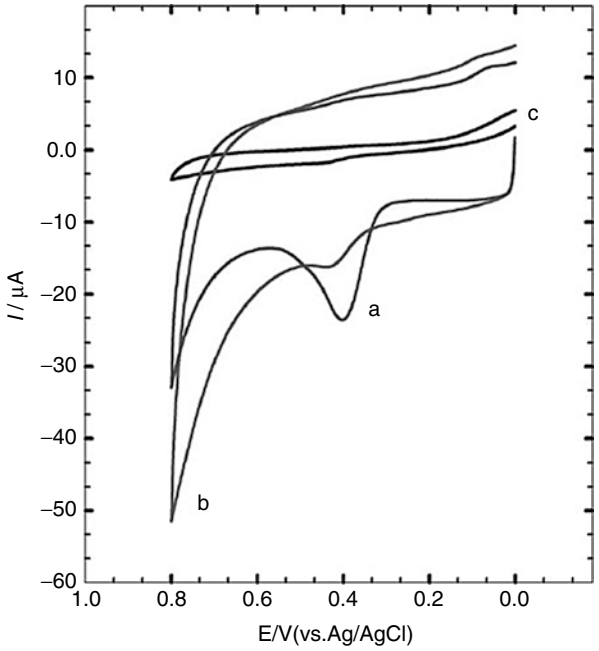

Fig. 19 Cyclic voltammograms of 5.0×10^{-4} mol L^{-1} morphine/ 0.1 mol L^{-1} BR, pH 7.4, at (*a*) PEDOT/Pt electrode in the presence of SDS, (*b*) PEDOT/Pt electrode (*c*) Pt electrode at scan rates 50 mV s^{-1} (Reprinted from [109], Copyright (2011), with permission from Elsevier)

reaction rate, and enhances greatly its anodic peak current (Fig. 19). PEDOT/Pt in the presence of SDS exhibited perfect electrocatalytic activity toward MO as it lowers its oxidation potential, enhances its current response, and improves its electron transfer kinetics. D_{app} (cm^2 s^{-1}) value for MO at PEDOT/Pt is 2.6×10^{-4} in the presence of SDS which is higher than the corresponding value in the absence of SDS 1.1×10^{-4}. The diffusion component of the charge transfer at the electrode surface is greatly affected by the anionic surfactant SDS [109].

On the other hand, DA is considered one of the most common interferents for MO in urine or blood. Two well-resolved peaks for DA and MO were obtained at 220 and 410 mV at PEDOT/Pt in the presence of SDS, respectively. The proposed sensor can determine MO in the presence of DA with high sensitivity and excellent peak potential separation (190 mV). Moreover, the simultaneous sensitive determination of MO and epinephrine EP was achieved well at the proposed sensor. Therefore, this promising sensor can be used to selectively and sensitively discriminate MO from neurotransmitters. Also, the simultaneous determination of MO, AA, and UA proved excellent at the proposed sensor. By the addition of SDS, the MO oxidation current increased, and the AA and UA oxidation current disappeared. This is attributed to the electrostatic attractions between the positively charged MO and negatively charged SDS and the electrostatic repulsion between the negatively charged AA and UA and anionic SDS [109]. On the other hand, MO can be discriminated

from codeine that is very close to MO in structure at the surface of the proposed sensor. Codeine usually interferes with MO and affects the MO determination because of the competitive adsorption between them. At the surface of the proposed sensor, no interference was detected from codeine in a solution containing equimolar amounts of MO and codeine in the presence of SDS. Only an oxidation peak for MO was detected at 550 mV. As a result, PEDOT/Pt in the presence of SDS can be used to detect MO in opium poppy in the presence of high concentration of codeine (ten-fold) [109].

As well, electrochemical impedance spectroscopy (EIS) is a characteristic tool that can be used to examine the electrode/solution interface properties. It also can be used to examine the type of interaction of MO at the proposed sensor in the absence and presence of SDS. The diameter of the semicircle in the Nyquist plot resembles the resistance of the electron transfer. In the absence of SDS, a semicircle with larger diameter was observed which is diminished obviously by SDS addition. As a result, the resistance of electron transfer of MO electrooxidation decreases, and electron transfer kinetics is improved. The fitting values calculated from the equivalent circuit for the impedance data were summarized in Table 4. R_u is the solution resistance, R_p is the polarization resistance, CPE is the predominant diffusion influence on the charge transfer process, and n is its corresponding exponent ($n<1$). C_f is the capacitance of the double layer. W is the Warburg impedance due to diffusion. The capacitive component values are higher at PEDOT/Pt in the presence of SDS compared to the case of the absence of SDS because of the ionic adsorption at the electrode surface, the charge transfer process, and the conducting character of the surface. In selective electrostatic interactions between MO and SDS, the accelerated electron transfer kinetics resulted in the obvious decrease in the interfacial electron transfer resistance [109].

Also, the voltammetric behavior of isoniazid (an antituberculous drug, INH) was investigated at PEDOT/Pt in the presence and absence of SDS and CTAB. INH exhibited a very weak electrochemical response at bare Pt electrode which was markedly enhanced in the presence of SDS achieving an improved response of INH in pH 2.3 (INH is positively charged in this pH). Two well-defined irreversible anodic peaks of INH were obtained at 630 mV and 820 mV (Fig. 20a) that resulted to form an irreversible oxidation of INH. In the absence of SDS, no peaks were obtained for INH due to electrostatic repulsion between the positively charged INH

Table 4 Summary of the data obtained from EIS in the determination of MO using PEDOT/Pt electrode in the absence and presence of SDS at the oxidation potential (Reprinted from [109], Copyright (2011), with permission from Elsevier)

Electrode PEDOT/Pt	E (mV)	R_p (kΩ cm^2)	R_u (kΩ cm^2)	C_f (μF cm^{-2})	W ($K\Omega^{-1}$ cm^{-2})	C_{CPE} (μF cm^{-2})	n
In the absence of SDS	420	122	0.39	45	2.49	75	0.88
In the presence of SDS	420	52	0.5	50	2.38	279.8	0.7

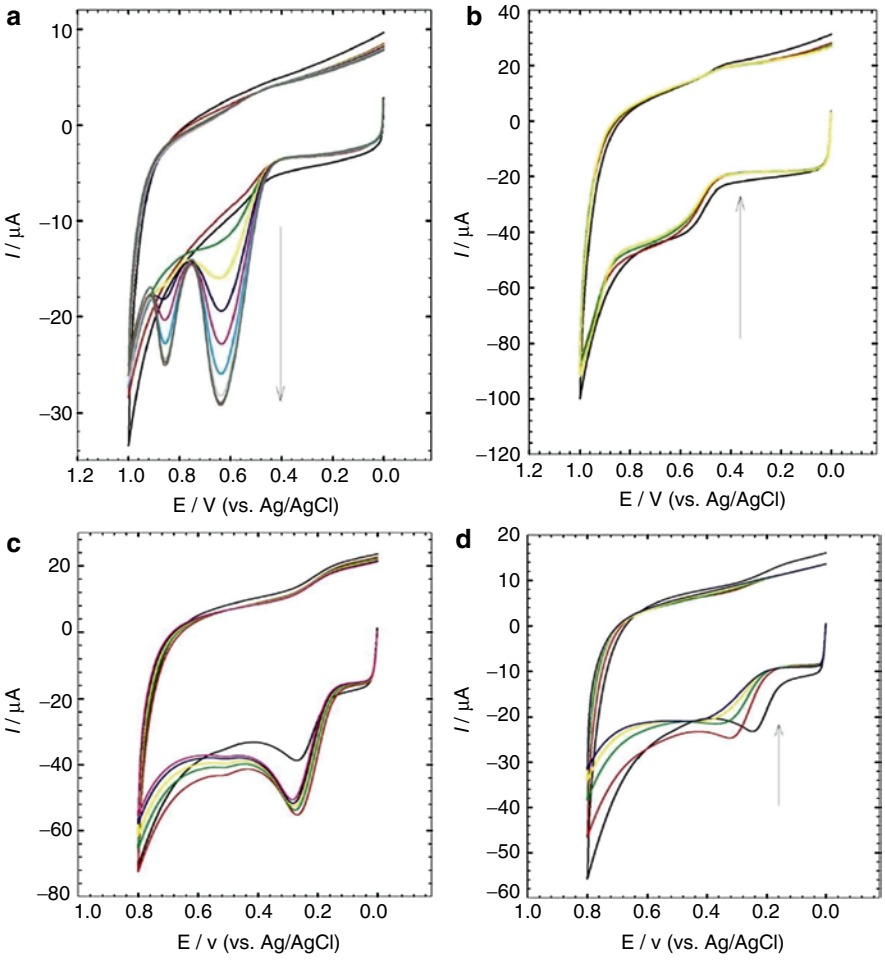

Fig. 20 Cyclic voltammograms of 5.0×10^{-4} mol L INH/0.1 mol L^{-1} L B-R, scan rate 50 mV s^{-1} at PEDOT/Pt electrode at pH 2.3 with successive additions (0–150 µL) of 0.1 mol L^{-1} (**a**) SDS, (**b**) CTAB and at pH 7.4 with successive additions (0–150 µL) of 0.1 mol L^{-1} (**c**) CTAB and (**d**) SDS (Reprinted from [110], Copyright (2011), with permission from Elsevier)

and positive charge density of PEDOT. SDS improves the oxidation current of INH and mediates the electron transfer kinetics as it facilitates the arrival of cationic INH to the electrode surface faster. Also, PEDOT/Pt in the presence of SDS exhibited high electrocatalytic activity toward INH showing lower oxidation potential and higher oxidation current [110]. On the other hand, a weak broad peak is observed at PEDOT/Pt in the presence of CTAB for INH solution/pH 2.3. By the addition of CTAB, the INH oxidation current decreases (Fig. 20b) due to the electrostatic repulsion between the cationic CTAB and the positively charged INH resulting in a retarded diffusion.

On the other hand, the electrochemical response of INH at pH 7.4 was studied at PEDOT/Pt in the presence of SDS and CTAB. INH becomes neutral at pH 7.4 according to its pK_a value resulting in different types of interaction of INH with the polymer film and surfactant molecules. At PEDOT/Pt, one oxidation peak for INH appeared at 260 mV with a current value of 38 μA because INH becomes neutral and diffuses easier toward the cationic polymer. By CTAB additions, the INH oxidation current increases to 55 μA then becomes stable (Fig. 20c). There are electrostatic force between INH molecules and CTAB resulting in enhanced oxidation current as the INH approaches the electrode surface faster and the reaction becomes easier. Figure 20d showed the opposite manner by the addition of anionic SDS; the INH oxidation current decreases because of the electrostatic force between INH and SDS resulting in difficult diffusion of INH to electrode surface [110]. Moreover, it is necessary to examine the simultaneous determination of INH, AA, and UA. At PEDOT/Pt in the presence of SDS, the selective determination of INH, AA, and UA at pH 2.3 proved excellent. This is attributed to the electrostatic attractions between anionic SDS and positively charged INH and electrostatic repulsions between SDS and anionic AA and UA. Also, the simultaneous determination of IHN, AA, and UA at pH 7.4 achieved well at PEDOT/Pt in presence of CTAB. Two oxidation peaks for AA and UA were observed at 100 and 486 mV, respectively, as a result of electrostatic attractions between cationic CTAB and anionic AA and UA. The oxidation current of INH is firstly observed at 700 mV and increased by the addition of CTAB as a result of INH neutral structure which improves its diffusion toward the polymeric film by CTAB. One can say that the presence of surfactant molecules plays a crucial role in the electrostatic interactions of INH toward the polymeric film in different pH values [110].

On the other hand, the electrochemical response of 0.3 mM atropine in 0.1 M B-R/ pH 7.4 was examined at PEDOT/Pt in SDS. One well-resolved irreversible peak was observed at 670 mV for atropine at PEDOT/Pt in the presence of SDS which was four and eight times higher than that observed at PEDOT/Pt and Pt electrodes, respectively. The oxidation current of atropine was markedly enhanced by the anionic SDS which mediates the approaching of atropine molecules to the electrode surface and facilitates the reaction. Higher current response, lower oxidation potential, and low detection limit of 34 nM were remarkable characteristics of the electrocatalytic activity of PEDOT/Pt toward atropine in the presence of SDS.

Also, an electroanalytical method was developed for the sensitive determination of flutamide in pharmaceutical formulations at polyglutamic acid polymer-modified carbon paste electrode in the presence of CTAB. The reduction current of flutamide increases by the addition of CTAB exhibiting a maximum 1 % CTAB and after that decreases continuously. The adsorption manner changes at 1 % CTAB from monomer adsorption to monolayer adsorption with an increase in CTAB concentration at the electrode surface. After 1 % CTAB, the reduction current decreases because of the retardation of electron transfer rate by micelle aggregates. Therefore, 1.0 % CTAB is selected as the optimum concentration. The proposed sensor showed perfect electrocatalytic activity toward flutamide determination, good sensitivity, excellent stability, and applicability with wide concentration range [111].

SAM of Surfactant on Polymers/Nanometallic Structures

Chunya Li et al. utilized gold nanoparticle-modified glassy carbon electrode (Au-NPs/GCE) for the determination of tryptophan (Trp) in the presence of sodium dodecylbenzenesulfonate (SDBS). The oxidation peak potential of Trp at Au-NPs/GCE showed a negative shift of 50 mV, and the peak current was improved in the presence of SDBS indicating that the electron transfer between the electrode and the bulk of solution was facilitated. Surfactants can be adsorbed on hydrophobic surface to form surfactant film altering the overvoltage of the electrode and influencing the rate of electron transfer [112]. In the presence of SDBS, a hydrophilic film with negative charge was formed through the interaction of Au-NPs and sulfonic group of SDBS. This hydrophilic layer improves the accumulation of Trp at the electrode surface through electrostatic interaction, thus the electron transfer of Trp was facilitated, its oxidation overpotential decreased, and its current response was enhanced [112]. Moreover, Gong-Jun Yang studied the electrochemistry of ethamsylate (ESL), a homeostatic agent that appears to maintain the stability of capillary walls and correct abnormal platelet adhesion, at hydrophobic gold nanoparticle-modified GCE ($C_{18}NH_2$-capped Nano-Au/GCE) in the presence and absence of cationic surfactant CTAB. A significant negative shift of the oxidation potential and increase of the anodic peak current were observed in the presence of CTAB indicating the role of CTAB in the oxidation of ESL. Sulfo acid group in ESL is ionized and negatively charged in the weak acid solution. In the presence of CTAB, a positively charged hydrophilic film of CTAB was formed on the modified surface. The hydrophobic interaction between ESL and hydrophobic chain of CTAB was more dominant than the static interaction with the polar head group, thus the overvoltage was reduced and the electron transfer rate was enhanced. Therefore, the electrochemical oxidation of ESL was facilitated in the presence of cationic surfactant CTAB, and very low detection limit was obtained, 3.5 nM [113].

Furthermore, the electrochemical response of DA was examined at Au/PEDOT–Au_{nano}/SDS (gold nanoparticle-modified PEDOT-modified gold electrode in the presence of SDS). This promising sensor combined the effective properties of PEDOT matrix to lower the DA oxidation potential and the catalytic properties of gold nanoparticles and SDS to facilitate the electron transfer kinetics (Fig. 21). The SDS addition improves the preconcentration–accumulation of hydrophobic positively charged DA, facilitates its diffusion through the modified electrode, and mediates the electrostatic transfer rate as a result of electrostatic interactions between cationic DA and anionic SDS leading to enhanced DA current signal at the proposed surface. The utilized sensor showed the effective synergism between PEDOT, Au_{nano}, and SDS to selectively and sensitively determine DA [27]. The previous results may be explained as follows: PEDOT matrix involves a distribution of reduced (hydrophobic) and oxidized (hydrophilic) regions, and positively charged DA tends to interact with the more reduced regions. In addition, PEDOT film acts as an electron facilitator as it contains a rich electron cloud. Furthermore, gold nanoparticles act as a mediator to facilitate the electrochemical reaction and mediate the electron transfer rate. Also, DA cations tend to be weakly adsorbed at

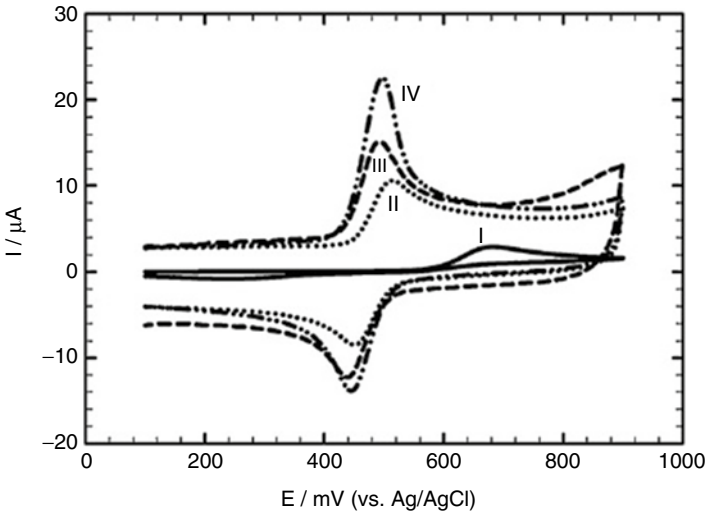

Fig. 21 CVs of 1 mmol L^{-1} DA/0.1 mol L^{-1} PBS/pH 2.58 at (*I*) bare Au, (*II*) Au/PEDOT, (*III*) Au/PEDOT–Au_{nano}, and (*IV*) Au/PEDOT–Au_{nano}/SDS-modified electrodes; scan rate 50 mV s^{-1} (Reprinted from [27], Copyright (2012), with permission from Elsevier)

Au/PEDOT–Au_{nano} as DA has the ability to form self-assembled monolayer on Au via the interaction NH_2 group of DA with Au. As mentioned before, SDS improves the preconcentration–accumulation of the positively charged DA at the surface of the modified electrode and enhances its diffusion through the modified electrode [27]. On the other hand, the simultaneous determination of AA, DA, and APAP (0.1 M PBS/ pH 2.58) achieved well at Au/PEDOT–Au_{nano} electrode. Three well-resolved peaks appeared at 0.235, 0.499, and 0.678 V for AA, DA, and APAP, respectively. By SDS addition, the anodic current of DA increased, the anodic current of AA diminishes, and the anodic current of APAP decreases slightly. The negative charge density of SDS film and the hydrophobic property of this film will act to enhance the preconcentration–accumulation of the hydrophobic DA^+ cations at the electrode surface and repel hydrophilic AA molecules away from the electrode surface. The anodic current of APAP decreased slightly by SDS addition because of its neutral structure in this pH resulting in slow diffusion toward electrode surface and retarded interaction with SDS. Furthermore, this promising sensor is used for the simultaneous determination of DA in the presence of AA and UA (0.1 M PBS/ pH 7.40). The oxidation peaks for UA, DA, and AA appeared at Au/PEDOT–Au_{nano} at 349 mV, 217 mV, and 19 mV, respectively, with large peak potential separation (Fig. 22, Scheme 6). By addition of SDS, the anodic current of DA increases, and the anodic current of AA and UA diminished. This is attributed to the electrostatic attraction between cationic DA and anionic SDS and electrostatic repulsion between anionic UA and AA and anionic SDS [27].

Au/PEDOT–Au_{nano}/SDS showed excellent stability which was examined through repeated cycles up to 50 cycles. Perfect stability was obtained at Au/PEDOT–Au_{nano}/

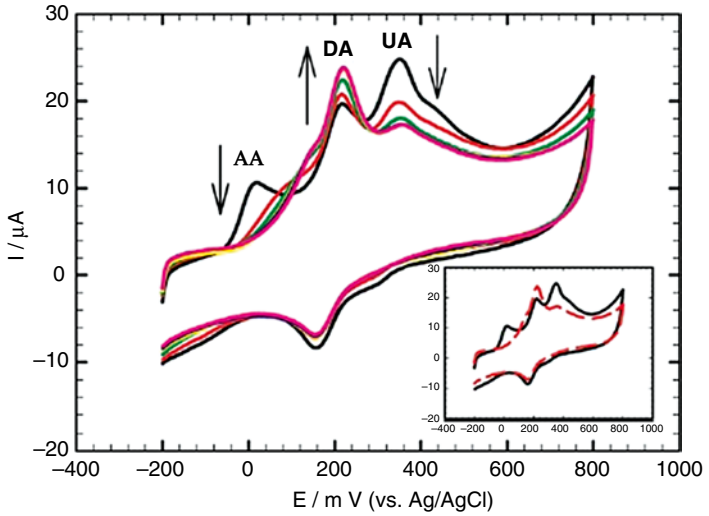

Fig. 22 CVs of tertiary mixture of 1 mmol L^{-1} AA, 0.5 mmol L^{-1} DA, and 0.5 mmol L^{-1} UA in 0.1 mol L^{-1} PBS/pH 7.40 at Au/PEDOT–Au_{nano}-modified electrode with successive additions of (0–200 μL) of 0.1 mol L^{-1} SDS; *inset* represents the initial (in the absence of SDS) and final (in the presence of 200 μL SDS) CVs; scan rate 50 mV s^{-1} (Reprinted from [27], Copyright (2012), with permission from Elsevier)

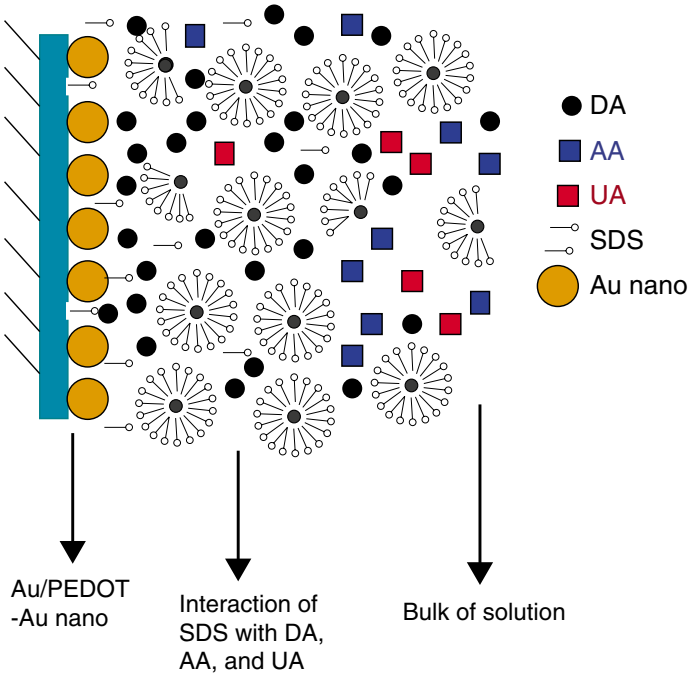

Scheme 6 Schematic diagram of interaction of DA, AA, and UA at Au/PEDOT/Au_{nano} in the presence of SDS

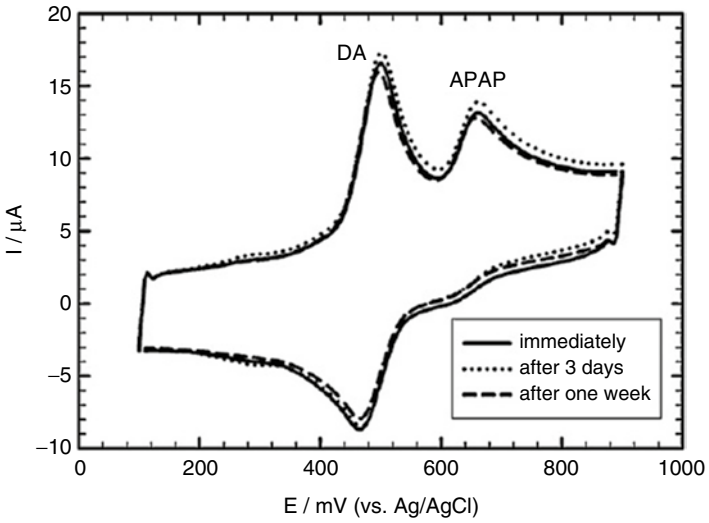

Fig. 23 CVs of the comparison of 50th cycle of long-term stability of Au/PEDOT–Au_{nano}. SDS for tertiary mixture (1 mmol L^{-1} AA, 1 mmol L^{-1} DA, and 1 mmol L^{-1} APAP/0.1 mol L^{-1} PBS/pH 2.58) separation immediately, after 3 days and 1 week of storage; scan rate 50 mV s^{-1} (Reprinted from [27], Copyright (2012), with permission from Elsevier)

SDS in 1 mmol L^{-1} DA/0.1 mol L^{-1} PBS/pH 2.58, and no decrease in the current response was observed. Furthermore, a very small peak separation was observed, nearly zero or 15 mV peak separation, which indicated the unusual reversibility obtained by repeated cycles. Moreover, long-term stability for the separation of a tertiary mixture of 1 mmol L^{-1} AA, 1 mmol L^{-1} DA, and 1 mmol L^{-1} APAP/0.1 mol L^{-1} PBS/pH 2.58 was examined at Au/PEDOT–Au_{nano}/SDS up to 1 week. The electrode is kept in 0.1 mol L^{-1} PBS/pH 2.58 in the refrigerator after each measurement. The CVs of the 50th cycle of repeated cycles of Au/PEDOT–Au_{nano}/SDS for tertiary mixture of AA, DA, and UA immediately after 3 days and 1 week of storage were shown in Fig. 23. The decrease of I_{pa} of DA and APAP was 6.7 % and 1.2 %, respectively, after 1 week of storage. Therefore, better stability via repeated cycles and long-term stability were obtained at Au/PEDOT–Au_{nano}/SDS not only for one component detection (DA) but also for tertiary mixture components separation [27].

Self-Assembled Monolayer of S-Containing Compounds on Nanostructures

SAMs formed by S-containing compounds, namely, thiols on gold–nanogold electrodes, are well-ordered, stable, and densely packed monolayers. They exhibit great characteristics like small overpotential, good sensitivity, perfect selectivity, reproducibility, and short response time in the electrocatalytic reactions. Moreover, the immobilized amount of S-functionalized compounds can be greatly increased by

their modifications with gold nanoparticles which further resulted in enhanced Au–S bond and enhancement of the SAMs stability. On the other hand, the sensory applications at SAM-modified metallic nanoparticle surface, namely, gold nanoparticles, in the presence of surfactants proved excellent and will be addressed in details.

Self-Assembled Monolayer

The design of electrodes with well-defined function and controllable surface properties can be effectively achieved by employing self-assembled monolayers (SAMs) of few nm to several hundred nm thickness [114, 115] of organic molecules (both aliphatic and aromatic) containing free anchor groups such as thiols, disulfides, amines, silanes, or acids [116, 117]. The advantages of SAMs include simplicity of preparation, versatility [118], extraordinary thermodynamic stability [119, 120], reproducibility, and the possibility of introducing different chemical functionalities with high level of order on a molecular dimension [121–127] providing an elegant approach to design tailored surfaces with controlled physical and chemical properties [128, 129]. In addition, several applications were allowed using SAM based on their terminal hydrophilic or hydrophobic functionality or by changing the chain length [115]. SAMs proved excellent in the immobilization of sensing elements like enzymes [118] and DNA. Also, they are very efficient in the electron transfer and capacitance control of an electrode [115]. SAMs can be described as an elegant method by which we can address electrically a molecular component [126, 127]. The method by which the SAMs were formed is the spontaneous adsorption of self-assembled molecules on metals like Au, Ag, Cu, Zn, Fe, Ni, glass, or Pt [130–132]. As well, highly organized [133], stable, and tightly packed compact monolayers can be formed on the electrode surface through the strong interchain and hydrophobic interactions (van der Wall interactions). As a result, various applications can be achieved like chemical sensing, protective coatings [128], lubricants [122], corrosion protection [128], patterning, semiconductor passivation, and optical second-order harmonic generation [134]. There are several reasons for the attractive features that SAMs are offering in biosensing applications:

(i) Miniaturization is very easy as SAMs utilize the bare minimum resources (a monolayer consisting of 10^{-7} mol/cm^2 or 10^{13} molecules/cm^2) [114].
(ii) The long-chain alkane thiols of SAMs that showed high degree of ordered and dense nature [114, 120] resulted in a microenvironment membrane which is efficient for the biological molecule immobilization.
(iii) The good chemical stability of SAMs even after its coupling with the immobilizing molecules for biological sensing makes SAMs efficient as biosensors and immunosensors [114].

Organosulfur compounds can form SAMs on metal substrate [116, 129] especially gold and the formed SAMs [135, 136]. This method is considered an effective method to prepare chemical interfaces that exhibited perfect features and

well-organized, structurally, well-defined, and stable resulting in SAMs having controllable thickness [137] and favorable function [118]. Organothiols lose the hydrogen of the thiol group [130] as molecular hydrogen H_2 upon chemisorption [138–143] on gold surface resulting in the formation of covalent, strong, and thermodynamically favored S–Au bond [144–146]. Thiols have great affinity to be adsorbed on gold due to the following:

(i) Inertness of gold; therefore, it does not form stable oxides on its surface.
(ii) The strong specific interaction of gold with sulfur resulting in stable monolayer formation [130, 131, 147] in a short time [141] and in a very reproducible way [131].

SAMs of thiols formed on gold electrodes are well-ordered, stable, and densely packed monolayers [131, 133]. They exhibit great characteristics like small overpotential, good sensitivity, perfect selectivity, reproducibility, and short response time in the electrocatalytic reactions [136, 148].

The electrochemical response at the SAM-modified electrode depends on the monolayer thickness. The "thick" monolayer (e.g., monolayers of long-chain alkanethiols) would passivate the electrode surface, and it slows down the electron transfer [137]. Also, the monolayer having hydrophilic functional groups can favor the permeation of ions in solution into the electrode surface, if any specific interaction exists at the monolayer solution interface. The SAMs having –COOH and –NH_2 functional groups are extensively used for electrochemical sensing applications and served as a platform for the fabrication of biosensors [134]. In recent years, more and more attention has been focused on L-cysteine (Cys) SAM-modified electrochemical sensors due to their good stability and highly characterized structures of the Cys SAM [149].

Methods of SAM Preparation

SAM can be prepared via two methods: immersion and electrochemical growth [114, 149]. The immersion growth is a common method for SAMs' formation through which the metal electrode is soaked in the required solution for a certain time then the electrode was washed with the same solvent and dried [114]. The substrate nature and roughness, type of solvent, adsorbate nature, adsorbate concentration, and temperature greatly affected the packing density and formation of SAMs. Very dilute solution gives ordered SAMs, while high concentration and long time (6 days) resulted in the formation of multilayer. Highly pure solvents such as water, ethanol, acetonitrile, and hexane are used to prepare solutions of thiol, sulfide, and disulfide [114]. The electrochemical growth was developed by Ying Zhuo et al. They reported that the immersion growth suffered from the competitive adsorption from other ions, for example, supporting electrolytes. In addition, the assemblies formed by immersion growth sometimes were subjected to nonuniform layer growth. The electrochemical method was free of the above drawbacks and more advantageous than immersion growth such as controllable and selective [149].

SAM-Modified Nanostructured Electrodes

SAM procedure opens a new avenue for the fabrication of electrodes having an electrocatalytic activity toward many electrochemical reactions superior to that of unmodified electrodes [150]. SAM-modified electrodes are very promising for the construction of electrochemical biosensors because they can enhance the electron transfer rate, selectivity, and sensitivity, improve the response time, and decrease the overpotential [151–153]. The SAM plays three important roles in the biosensing applications: (i) it forms thin monolayer, (ii) it forms weak hydrogen-bonding interactions, and (iii) it prevents fouling of the electrode surface by the oxidation products [137]. SAMs of thiol molecules on a metal surface provide a useful means of immobilizing electrode surfaces to attach various functional groups, such as nanoparticles and redox-active species [136].

Gold nanoparticles that are conjugated to globular protein, bovine serum albumin, through S–Au bond showed more surface area for strong interaction with the external species [154]. Furthermore, the modification using gold nanoparticles could greatly improve the S-functionalized compounds' immobilized amount, affect the SAM structure [155], enhance the Au–S bond, and improve the SAMs' layer stability [147]. The high surface energy of nanoparticles resulted in their instability; therefore, they need suitable surface modifications to be stabilized against aggregation. Cyano (CN), amino (NH_2), and mercapto (SH) are functional groups that exhibited great affinity toward gold. Hak Yong Kim identified the interaction of cysteine and gold nanoparticles and indicated that the cysteine thiol moiety is an effective site for gold interaction resulting in the formation of stable cysteine-capped gold nanoparticles. Gold nanoparticles were stabilized by cysteine molecules through S–Au interaction [45]. Figure 24a displayed the TEM image of spherical gold nanoparticles with a corona of cysteine ligand. Moreover, the TEM confirmed the gold

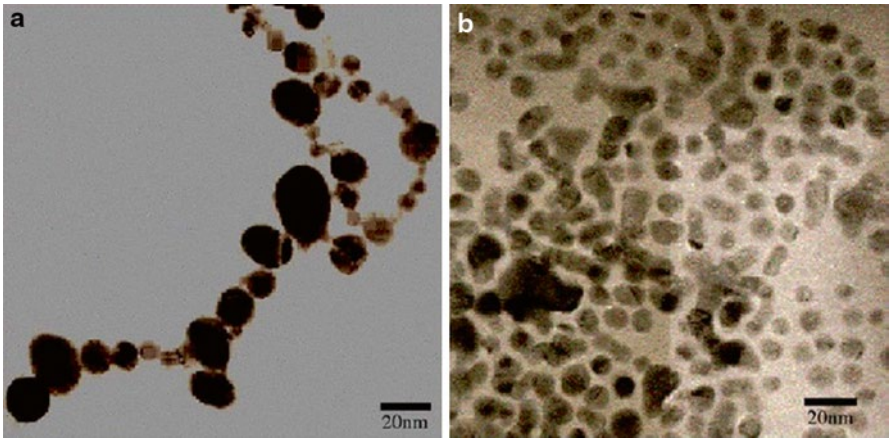

Fig. 24 TEM images of (**a**) cysteine-capped gold nanoparticles and (**b**) gold nanoparticles in gold hydrosol (Reprinted from [154], Copyright (2006), with permission from Elsevier)

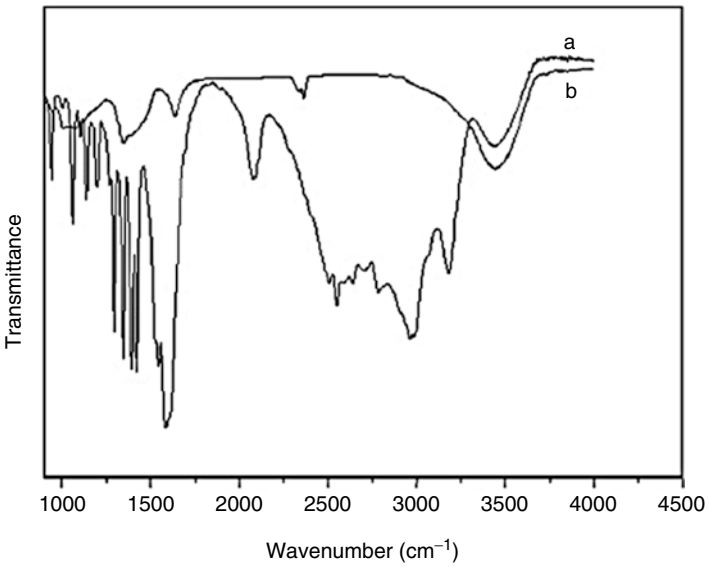

Fig. 25 Infrared spectra of cysteine (*spectrum a*) and cysteine-capped gold nanoparticles (*spectrum b*) (Reprinted from [154], Copyright (2006), with permission from Elsevier)

nanoparticles' stabilization because of their interaction with cysteine. Figure 24b showed the TEM image of the clusters of gold nanoparticles that are formed by $NaBH_4$ reduction. Moreover, the characteristic bands of cysteine moiety after gold nanoparticles' conjugation were detected through the application of FTIR spectra. Amino acids exhibit spectra characteristic of both carboxylate and primary amine salts as they can be described as zwitterions. The FTIR spectra of Cys and Cys/gold nanoparticles were shown in Fig. 25. The characteristics bands in Cys (spectra a) appeared at 1600, 1390 cm^{-1} for the asymmetric and symmetric stretching of COO^-, at 1532 cm^{-1} for *N*–H bending, the broad 3000–3500 cm^{-1} range for stretching NH_3^+, and near 2550 cm^{-1} for S–H group in the cysteine molecule. These results are very close to IR spectra of cysteine. The spectra of Cys/gold nanoparticles (spectra b) showed slight changes. A slight shift in COO^- and NH_3^+ stretching positions occurs because of the change in their dipole moment as a result of cysteine binding on the high electron density metal surface. Significantly, the S–H band was not observed in the spectra of Cys/gold confirming the Au–S bond [154].

Desorption of SAM

The formation of SAM of alkanethiols on bare gold and gold nanoparticle-modified electrode through the S–Au bond can be confirmed using the electrochemical desorption experiment. Alkanethiol monolayers on gold electrodes undergo oxidative and reductive desorption. The oxidative desorption of Au–Cys (a) and

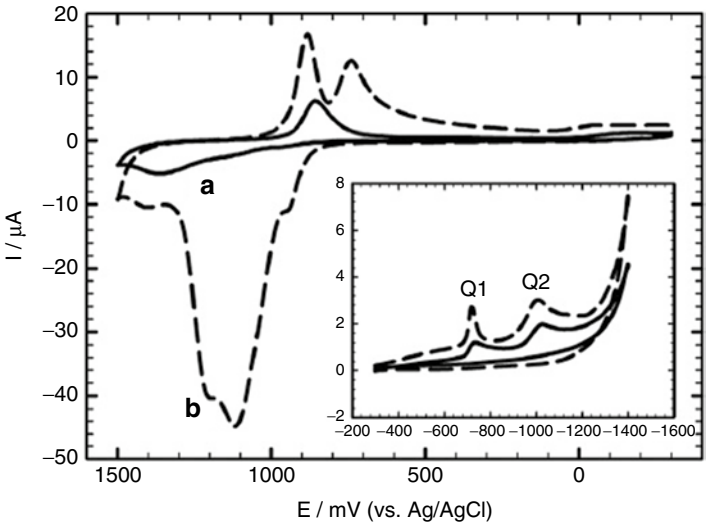

Fig. 26 CVs of the oxidative desorption of Au–Cys (*a*) and Au/Au_{nano}–Cys (*b*) in 0.1 mol L^{-1} PBS/pH 2.58, *inset*; CVs of the reductive desorption of Au–Cys (*solid line*) and Au/Au_{nano}–Cys (*dash line*) in 0.5 mol L^{-1} KOH; scan rate 50 mV s^{-1} (Reprinted from [31], Copyright (2012), with permission from Elsevier)

Au/Au_{nano}–Cys (b) electrodes in 0.1 mol L^{-1} PBS/pH 2.58 was shown in Fig. 26. From this figure, we can deduce that gold nanoparticles increase the assembly amount of cysteine and affect the SAM structure and stability. On the other hand, thiols undergo reductive desorption in alkaline solutions via a one-electron reduction reaction:

$$\mathbf{Au - SR + e^- \rightarrow Au^o + RS^-}$$

The amount of the charge consumed during the reductive desorption can be used to determine the surface concentration of the thiolates. The reductive desorption of Au–Cys (solid line) and Au/Au_{nano}–Cys (dash line) in 0.5 mol L^{-1} KOH was shown in the inset of Fig. 26. At bare gold electrode, two cathodic peaks are observed at −736 mV and −1027 mV, and at gold nanoparticle-modified electrode, cathodic peaks are at −720 mV and −1008 mV. As a result of gold nanoparticles' deposition, the desorption peak current increased largely. Wenrong Yang et al. indicated that the first peak (Q1) is attributed to the Au–S bond cleavage (having a shape characteristic of an adsorbed species), and the second peak (Q2) is attributed to a similar field-induced rearrangement of cysteine clusters which would occur within the electrical double layer (having more diffusion-like character). Therefore, the area under the first peak (Q1) can be used to determine the surface coverage of cysteine. The estimated surface coverage of cysteine SAM is 2.64×10^{-9} mol cm^{-2} and 4.43×10^{-9} mol cm^{-2} on bare gold- and gold nanoparticle-modified electrode, respectively. As a result, modification using gold nanoparticle can markedly improve the immobilization amount of cysteine and enhance the Au–S bond and stability of cysteine SAM [31, 155].

Sensing Applications of SAM-Modified Nanostructures

Binary SAM of 3-mercaptopropionic acid (MPA, HS–$(CH_2)_2$–COOH) and 1-tetradecanethiol (TDT, HS–$(CH_2)_{13}CH_3$) was formed on 2D bare gold (Au) and 3D Au-NP-modified electrode by Dong-Shik Kim. Electron transfer rate (k_{et}), charge transfer resistance (R_p), Warburg element (W_d), double layer capacitance (C_{dl}), and time constant exhibited significant changes of the binary SAM and uni-SAM formation on the bare gold and Au-NP surfaces. Greater k_{et} and C_{dl} were obtained in the case of a binary SAM of MPA and TDT on the Au-NP compared to that on the binary SAM on planar bare gold surface. This is due to the less ordering of binary SAM structure on the Au-NP than that on the planar Au electrode resulting in a reduced interaction between the SAM molecules on the Au-NP than that on the planar Au electrode. Moreover, the functional group affinity, COOH and CH_3, chain–chain interaction, hydrogen bonding, and Au-NPs surface curvature affect the stability and surface coverage of the SAM [115]. Moreover, gold electrodes modified with gold nanoparticles, cysteamine (CA) and 3-mercaptopropionic acid (MPA), was utilized for simultaneous determination of epinephrine EP, AA, and UA. The electron transfer rate of EP on the modified electrodes was enhanced compared to the bare electrode. The voltammetric response of EP at 2D- and 3D-modified gold templates, Au/MPA, Au/MPA/CA/Au-NPs, Au/Au-NPs, Au/Au-NPs/MPA, and Au/Au-NPs/MPA/CA/Au-NPs, respectively, were compared and showed in Fig. 27. Lower oxidation potential, higher oxidation current, and greater catalytic effect were achieved for EP at modified electrodes prepared on 3D template compared to that on 2D gold template. The 3D layer may provide better curvature and therefore better penetration of EP through the alkane chains on nanoparticle surface compared to the 2D layers. As a result, the electron transfer kinetics of EP and the electrode surface is better on 3D MPA layers compared to 2D MPA layers [147]. On the other hand, a promising electrochemical sensor of Au/Au_{nano}–Cys/SDS for DA [156] and EP [31] was constructed through the formation of SAM of cysteine on gold nanoparticle-modified gold electrode. The electrochemistry of DA at different modified electrodes (Au/Au_{nano}, Au/Au_{nano}/SDS, Au/Au_{nano}–Cys, and Au/Au_{nano}–Cys/SDS) was displayed in Fig. 28 and Table 3. The electrochemistry of DA at Au/Au_{nano} (Au electrode modified with gold nanoparticles) showed a great current response (I_{pa} = 5.6 μA), low oxidation potential (E_{pa} = 516 mV), and enhanced reversibility (ΔE_p = 45 mV) Fig. 28 (I). These observations are attributed to the catalytic effect of Au_{nano} that act as a facilitator to improve the electron transfer rate and enhance the electrochemical reaction. By the addition of 160 μL of SDS at Au/Au_{nano}, the oxidation current of 1 mmol L^{-1} DA in 0.1 mol L^{-1} PBS/pH 2.58 decreased from 5.6 μA at Au/Au_{nano} to 4.2 μA at Au/Au_{nano}/SDS Fig. 28 (II). There is an interaction between Au_{nano} and SDS through SDS hydrophobic long carbon chain that resulted in the blocking of the binding sites on gold nanoparticles. This SDS layer acts as an insulating layer rather than enhancing the charge transfer, thus the oxidation current of DA decreases in the presence of SDS. On the other hand, the CV of DA at Au/Au_{nano}–Cys (cysteine SAM-modified Au_{nano}-modified gold electrode) was shown in Fig. 28 (III). The oxidation current of DA decreased from 5.6 μA to 3 μA,

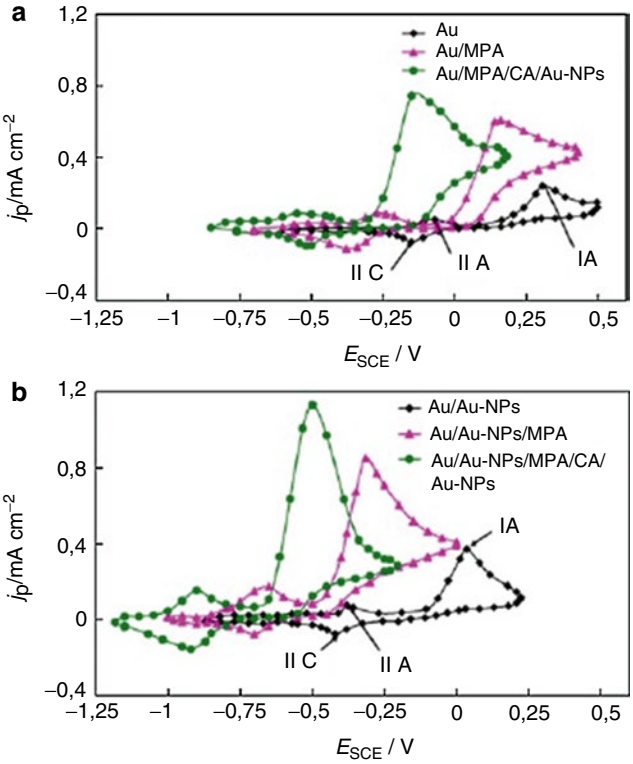

Fig. 27 (**a**) Cyclic voltammograms of the Au electrode, Au/MPA, and Au/MPA/CA/Au-NP-modified gold electrodes and (**b**) cyclic voltammograms of the Au-NPs, Au/Au-NPs/MPA, Au/Au-NPs/MPA/CA/Au-NP-modified gold electrodes in 60 mM phosphate buffer (pH 7) with 500 μM epinephrine. v = 0.1 Vs^{-1} (Reprinted from [147], Copyright (2009), with permission from Elsevier)

the oxidation potential was shifted from 516 mV to 586 mV, and the peak separation increased from 45 mV to 148 mV by the modification with Cys SAM. These observations were attributed to the (i) cysteine molecules' disorganization on gold nanoparticles resulting in the inhibition of hydrogen bond formation between DA and cysteine and (ii) electrostatic repulsion between the positively charged cysteine (it is a zwitterionic amino acid and its isoelectric point is 5.06; if the pH of electrolyte is lower than 5.06, the amino group of cysteine is protonated and cysteine is positively charged) and the cationic DA resulting in the hindrance of DA molecules from reaching the electrode surface, decrease of the oxidation current, and increase of the potential peak separation.

The electrochemistry of DA at cysteine SAM-modified Au_{nano}-modified gold electrode in the presence of 40 μL SDS was shown in Fig. 28 (IV) (Au/Au_{nano}–Cys/SDS). In the presence of 40 μL SDS, the oxidation current increased from 3 μA to 4.3 μA, the oxidation potential was shifted from 586 mV to 504 mV, and the peak separation

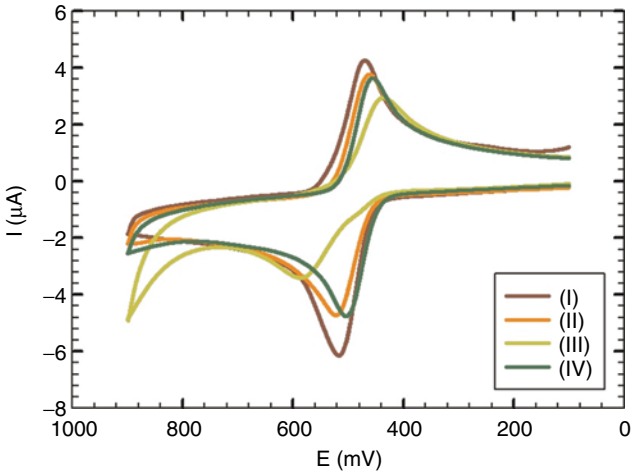

Fig. 28 CVs of 1 mmol L^{-1} DA at (*I*) Au/Au_{nano}, (*II*) Au/Au_{nano}/SDS, (*III*) Au/Au_{nano}–Cys, and (*IV*) Au/Au_{nano}–Cys/SDS-modified electrodes; scan rate 50 mV s^{-1} (Reprinted from [156], Copyright (2012), with permission from Elsevier)

decreased from 148 mV to 47 mV. As mentioned before, there is an electrostatic repulsion between cationic DA and cationic cysteine layer. The addition of SDS (an anionic surfactant) improves the DA diffusion through the cationic cysteine layer because of the electrostatic attractions between the anionic SDS and cationic DA (Scheme 7). Moreover, there is an electrostatic attraction between anionic SDS and the positively charged cysteine SAM which allows cysteine molecules' reorganization on gold nanoparticles, improving the formation of the hydrogen bond between DA and cysteine and promoting faster the rate of the electron transfer. An increase of the oxidation current, higher electron transfer rate, smaller peak separation, and better reversibility were observed for DA [156] and EP at Au/Au_{nano}–Cys/SDS. Table 5 showed the CVs of DA at Au–Cys and Au/Au_{nano}–Cys, we can deduce that the cysteine effect on the polycrystalline bare Au response is more pronounced than that on gold nanoparticles and its effect on gold nanoparticles is enhanced by using SDS. SDS promotes the cysteine reorganization on gold nanoparticles resulting in enhanced oxidation current, small peak separation, and better reversibility. The peak potential separation ($\Delta E_p \sim 45$ mV) was the same in the cases of Au/Au_{nano} and Au/Au_{nano}–Cys/SDS indicating the high reversibility and the strong adsorption of the electroactive species at the electrode surface. Au/Au_{nano} displays a little higher current response, but Au/Au_{nano}–Cys/SDS shows, besides the high current response, better stability through repeated cycles and long-term stability.

In addition, the diffusion coefficient (D_{app}) values for DA and EP were 5.00×10^{-6} and 1.24×10^{-5} cm^2 s^{-1} at Au/Au_{nano}–Cys and 1.06×10^{-5} and 3.86×10^{-5} cm^2 s^{-1} at Au/Au_{nano}–Cys/SDS, respectively. The charge transfer diffusion component at Au/Au_{nano}–Cys was affected markedly by the anionic SDS. The D_{app} values showed that

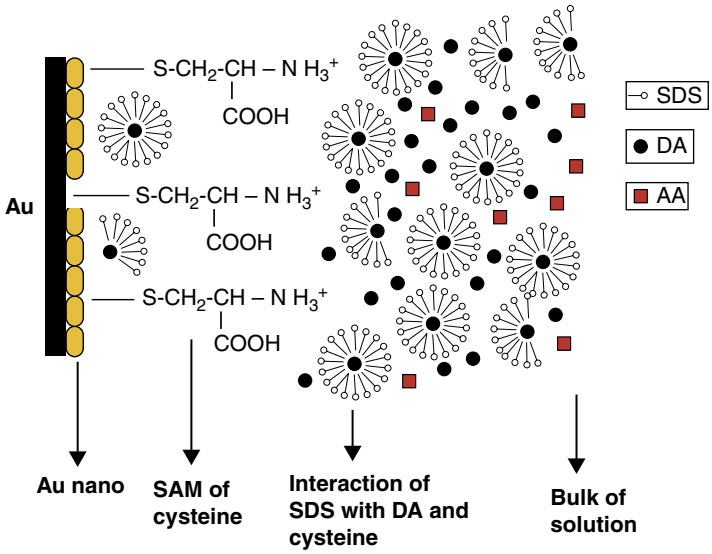

Scheme 7 Schematic model of Au/Au_{nano}–Cys/SDS-modified electrode in the presence of DA cations and AA (Reprinted from [156], Copyright (2012), with permission from Elsevier)

Table 5 CV results for the redox reaction of 1 mmol L^{-1} DA/0.1 mol L^{-1} PBS/pH 2.58 at different modified electrodes (Au, Au–Cys, Au/Au_{nano}, Au/Au_{nano}/SDS, Au/Au_{nano}–Cys, and Au/Au_{nano}–Cys/SDS (Reprinted from [156], Copyright (2012), with permission from Elsevier)

Electrode	E_{pa} (mV)	I_{pa} (μA)	E_{pc} (mV)	I_{pc} (μA)	ΔE_p (mV)
Au	683	2.82	235	0.478	448
Au–Cys	636	2.55	379	2.14	257
Au/Au_{nano}	516	5.57	471	4.56	45
Au/Au_{nano}/SDS	522	4.20	462	4.24	60
Au/Au_{nano}–Cys	586	2.99	438	3.24	148
Au/Au_{nano}–Cys /SDS	504	4.35	457	3.99	47

DA and EP diffusion on Au/Au_{nano}–Cys was improved in the presence of SDS rather than in the absence of it [31, 156]. On the other hand, simultaneous determination of tertiary mixture of AA, DA [156] or EP [31], and APAP was examined at this modified electrode. The DPVs of tertiary mixture of 1 mmol L^{-1} AA, 1 mmol L^{-1} DA, and 1 mmol L^{-1} APAP in 0.1 mol L^{-1} PBS/pH 2.58 at Au/Au_{nano}–Cys with successive additions of 0–40 μL of 0.1 mol L^{-1} SDS was shown in Fig. 29. At Au/Au_{nano}–Cys, three well-resolved oxidation peaks appeared at 300, 468, and 648 mV for AA, DA and APAP, respectively. By SDS addition, the DA and APAP oxidation current increases, while the AA oxidation current diminishes. The negatively charged SDS film besides the hydrophobic character of the interior of this film resulted in the repulsion of the hydrophilic AA molecules away from the electrode

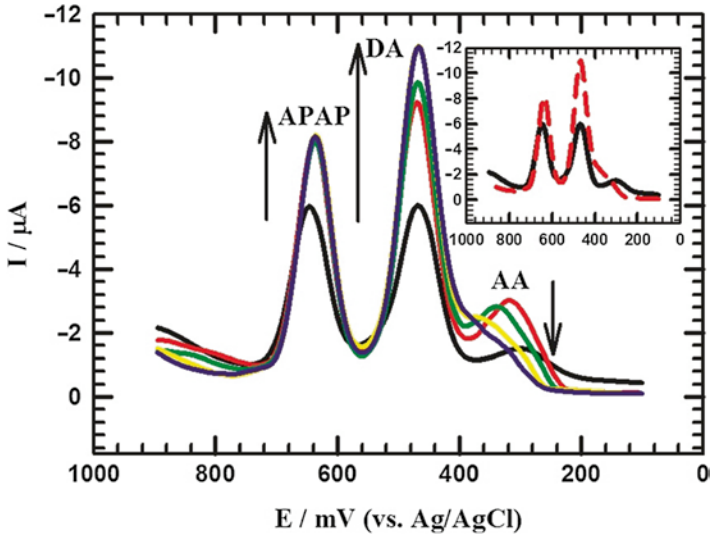

Fig. 29 Differential pulse voltammograms for 1 mmol L^{-1} AA, 1 mmol L^{-1} DA, and 1 mmol L^{-1} APAP in PBS (0.1 mol L^{-1}) at Au/Au_{nano}–Cys with successive additions of (0–40 μL) of 0.1 mol L^{-1} SDS at pH 2.58; the *inset* represents the initial (in the absence of SDS) and final (in the presence of 40 μL SDS) DPVs (Reprinted from [156], Copyright (2012), with permission from Elsevier)

surface while enhancing the preconcentration–accumulation of hydrophobic cations of DA and APAP. The negatively charged SDS that adsorbed onto the electrode surface has the ability to control the electrode reactions of AA, DA or EP, and APAP that differ in their net charge [31, 156]. Furthermore, Au/Au_{nano}–Cys/SDS was utilized for the simultaneous determination of binary mixture of EP and APAP (0.1 M PBS/pH 7.40) (inset of Fig. 30). Two well-defined peaks appeared at 222 mV and 431 mV for EP and APAP at Au/Au_{nano}–Cys, respectively. By SDS addition, EP oxidation peak current increased as a result of electrostatic interaction of the anionic SDS with the cationic EP, while the oxidation current of APAP decreased due to its neutral structure [31]. Also, Au/Au_{nano}–Cys/SDS can selectively determine EP in the presence of a large amount of UA and glucose (PBS/pH 7.40) (Fig. 30). No interference was observed from glucose at the modified electrode. At Au/Au_{nano}–Cys, two well-defined peaks appeared: 212 mV and 418 mV for EP and UA, respectively. By SDS addition, EP oxidation peak current increased, and UA oxidation peak current decreased due to the electrostatic interactions (attraction and repulsion, respectively) with anionic SDS. Furthermore, low detection limit of 0.294 nmol L^{-1} and quantification limit of 0.981 nmol L^{-1} for EP were obtained at Au/Au_{nano}–Cys/SDS [31]. Moreover, the physical morphology of the surface can be used to explain the electrochemical responses of different sensors. Figure 31a showed the SEM image of gold nanoparticles which are located at different elevations and homogenously distributed exhibiting large surface area. Figure 31d showed the SEM image of gold nanoparticles modified with SDS; the nanoparticles have dendritic shape with different sizes and are randomly distributed on the surface. Also, a

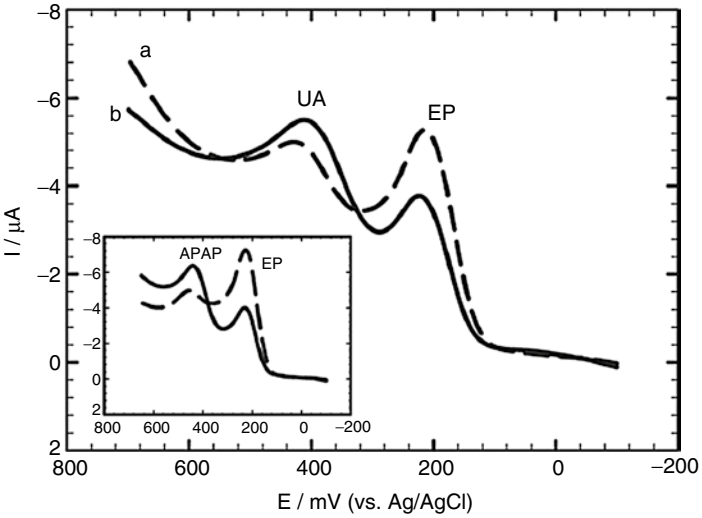

Fig. 30 Linear sweep voltammograms (LSVs) of 0.5 mmol L^{-1} EP, 1 mmol L^{-1} UA in the presence of 5 mmol L^{-1} glucose in 0.1 mol L^{-1} PBS/pH 7.40 at (*a*) Au/Au_{nano}–Cys and (*b*) Au/Au_{nano}–Cys/SDS, *inset*; LSVs of 1 mmol L^{-1} EP, 1 mmol L^{-1} APAP/0.1 mol L^{-1} PBS/pH 7.40 at Au/Au_{nano}–Cys (*solid line*) and Au/Au_{nano}–Cys/SDS (*dash line*); scan rate 50 mV s^{-1} (Reprinted from [31], Copyright (2012), with permission from Elsevier)

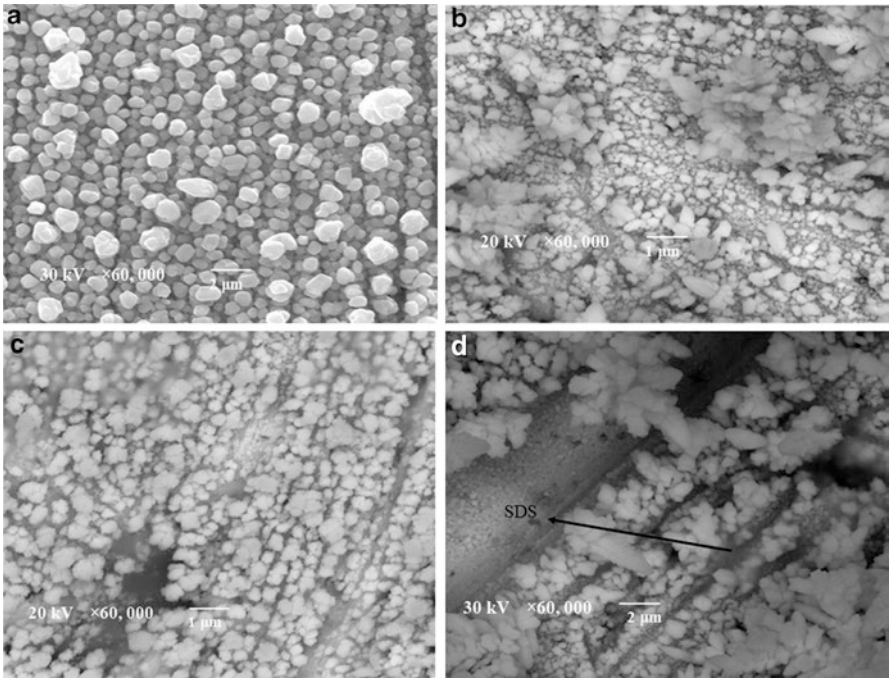

Fig. 31 SEM images of (**a**) Au/Au_{nano}, (**b**) Au/Au_{nano}–Cys, (**c**) Au/Au_{nano}–Cys/SDS, and Au/Au_{nano}/SDS electrodes (Reprinted from [31], Copyright (2012), with permission from Elsevier)

Table 6 CV results for the 1st, 25th, and 50th cycles of the repeated cycle stability of Au/Au_{nano}–Cys electrode in 1 mmol L^{-1} DA/0.1 mol L^{-1} PBS/pH 2.58

Cycle	I_{pa} (μA)	E_{pa} (mV)	I_{pc} (μA)	E_{pc} (mV)	ΔE_p (mV)
1st	2.46	585	2.63	465	120
25th	3.87	480	3.16	480	zero
50th	3.84	480	3.13	480	zero

spongy film is observed due to the surfactant film on the surface acting as an insulating layer rather than enhancing the charge transfer, thus, the oxidation current of DA at gold nanoparticles surface decreases in the presence of SDS. Figure 31b showed the SEM image of gold nanoparticles modified with cysteine SAM; the nanoparticles have dendritic shape with different sizes and are randomly distributed on the surface. Figure 31c showed the SEM image of gold nanoparticles modified with cysteine SAM and further modified with SDS; the nanoparticles are better dispersed, highly packed, and homogenously distributed on the surface. Reorganization and redispersion of gold nanoparticles occur as a result of the electrostatic attraction between the anionic SDS and cationic cysteine. A spongy film is observed in Fig. 31c due to the surfactant film on the surface [31, 156]. Furthermore, the stability of the different modified electrodes was studied via repeated cycles up to 50 cycles. Au/Au_{nano}, Au/Au_{nano}/SDS, Au/Au_{nano}–Cys, and Au/Au_{nano}–Cys/SDS electrodes in 1 mmol L^{-1} DA/0.1 mol L^{-1} PBS/pH 2.58 exhibited excellent stability with no current response decrease. These modified electrodes exhibited good reproducibility and do not suffer from surface fouling during the repetitive voltammetric measurement. The bare Au electrode exhibited bad stability because of the electrode fouling. On the other hand, very small peak potential separation (~ zero or 15 mV) was obtained indicating unusual high reversibility at the surface of these modified electrodes. From the CV that compared the 1st, 25th, and 50th cycles of repeated cycles stability of Au/Au_{nano}–Cys electrode, it was found that I_{pa} increased from 2.5 μA in the 1st cycle up to 3.8 μA in the 25th and 50th cycles and the peak separation decreased from 120 mV in the 1st cycle to ~0 mV in the 25th and 50th cycles (Table 6). These observations indicate that cysteine molecules undergo reorganization on gold nanoparticles resulting in mediation of DA diffusion through the electrode surface and enhancement of the hydrogen bonding between the hydrogen in hydroxyl–phenol of DA and the nitrogen in the L-Cys which enhances the electron transfer rate of DA molecules. Therefore, cysteine molecules undergo reorganization on gold nanoparticles by repeated cycles or by SDS addition (instantaneous reorganization).

Moreover, the long-term stability of Au/Au_{nano}, Au/Au_{nano}–Cys, and Au/Au_{nano}–Cys/SDS electrodes was studied up to 1 week (Tables 7 and 8). The electrode is kept in 0.1 mol L^{-1} PBS/pH 2.58 in the refrigerator after each measurement. The repeated cycles of Au/Au_{nano} and Au/Au_{nano}–Cys/SDS electrodes after 1 week of storage were shown in Fig. 32a, b, respectively. I_{pa} of the 50th cycle decreased by 26 % and 44 %, and the peak separation increased to 120 mV and 180 mV after 3 days and 1 week of storage, respectively, in the case of Au/Au_{nano} electrode. In addition, I_{pa} of the 50th cycle decreased by 23.6 % and 35.6 %, and the peak separation was zero and 15 mV after the same periods of storage, respectively, in

Table 7 CV results for the 50th cycle of the repeated cycle stability of Au/Au_{nano}, Au/Au_{nano}–Cys, and Au/Au_{nano}–Cys/SDS electrodes in 1 mmol L^{-1} DA/0.1 mol L^{-1} PBS/pH 2.58 immediately

Electrode	E_{pa} (mV)	I_{pa} (μA)	E_{pc} (mV)	I_{pc} (μA)	ΔE_p (mV)
Au/Au_{nano}	480	3.54	480	3.14	zero
Au/Au_{nano}–Cys	480	3.84	480	3.13	zero
Au/Au_{nano}–Cys/SDS	495	3.53	480	3.07	15

Table 8 CV results for the 50th cycle of the repeated cycle stability of Au/Au_{nano}, Au/Au_{nano}–Cys, and Au/Au_{nano}–Cys/SDS electrodes in 1 mmol L^{-1} DA/0.1 mol L^{-1} PBS/pH 2.58 after 1 week of storage

Electrode	E_{pa} (mV)	I_{pa} (μA)	E_{pc} (mV)	I_{pc} (μA)	ΔE_p (mV)
Au/Au_{nano}	585	1.97	405	1.51	180
Au/Au_{nano}–Cys	495	2.47	480	2.40	15
Au/Au_{nano}–Cys/SDS	525	2.69	465	2.57	60

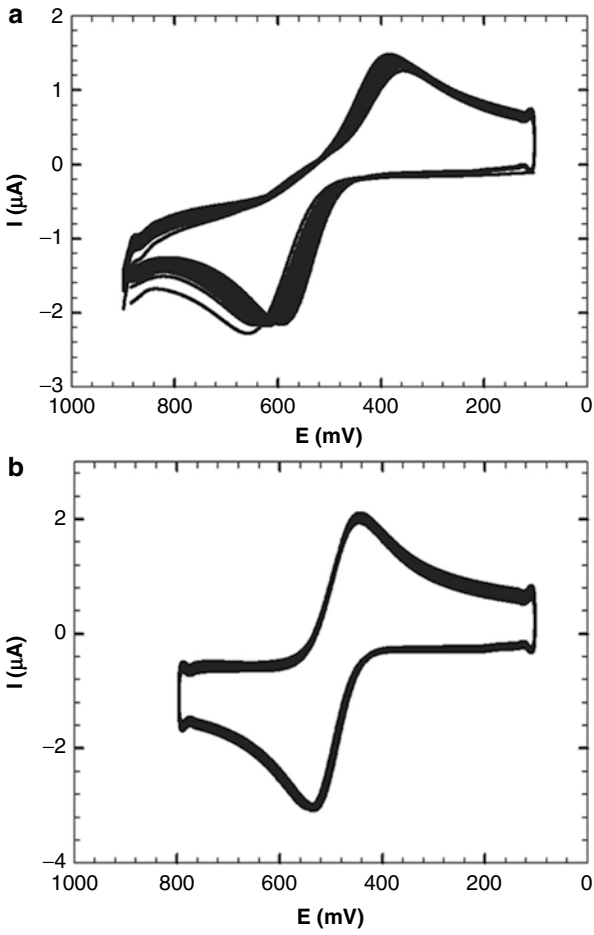

Fig. 32 Long-term stability of (**a**) Au/Au_{nano} and (**b**) Au/Au_{nano}–Cys/SDS (40 μL) after 1 week, 50 repeated cycles, 50 mV s^{-1} scan rate (Reprinted from [156], Copyright (2012), with permission from Elsevier)

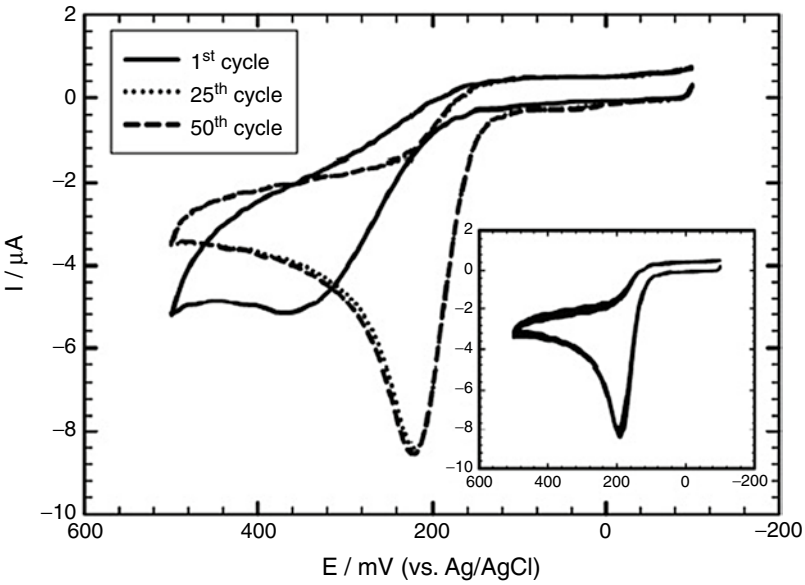

Fig. 33 Comparison of 1st, 25th, and 50th cycles of repeated cycle stability of Au/Au_{nano}–Cys electrode in 1 mmol L^{-1} EP/0.1 mol L^{-1} PBS/pH 7.40. *Inset*: CV of repeated cycles stability of Au/Au_{nano}–Cys/SDS-modified electrode in 1 mmol L^{-1} EP; scan rate 50 mV s^{-1} (Reprinted from [31], Copyright (2012), with permission from Elsevier)

the case of Au/Au_{nano}–Cys electrode. Also, I_{pa} decreased by 24 %, and the peak separation was 15 and 60 mV after 3 days and 1 week of storage, respectively, in the case of Au/Au_{nano}–Cys/SDS electrode (Tables 7 and 8).

These results confirmed that the presence of cysteine SAM on gold nanoparticles improved the reversibility and the long-term stability of Au/Au_{nano}–Cys and Au/Au_{nano}–Cys/SDS electrodes due to the formation of strong Au–S bond [156].

On the other hand, excellent stability of Au/Au_{nano}–Cys electrode for mixture separation (AA, DA, and APAP) in the presence of SDS was achieved via repeated cycling up to 50 cycles. As well, the long-term stability for the separation of AA, DA, and APAP tertiary mixture on Au/Au_{nano}–Cys electrode was studied in the presence of SDS. I_{pa} of DA decreased by 14 % and 17 % and I_{pa} of APAP decreased by 15 % and 28 % after 3 days and 1 week of storage, respectively. In addition, the long-term stability for the separation of the same mixture at Au/Au_{nano} electrode was studied. I_{pa} of DA decreased by 34 % and 44 % and I_{pa} of APAP decreased by 9 % and 33 % after 3 days and 1 week of storage, respectively. Therefore, Au/Au_{nano}–Cys in the presence of SDS exhibited a better stability via repeated cycles and longer-term stability not only for one component detection but also for tertiary mixture separation [156].

Furthermore, the same study was utilized in EP at the different modified electrodes via repeated cycles up to 50 cycles. The repeated cycle stability of the Au/Au_{nano}–Cys/SDS-modified electrode was shown in the inset of Fig. 33. Au/Au_{nano}–Cys and

Au/Au_{nano}–Cys/SDS-modified electrodes in 1 mmol L^{-1} EP/0.1 mol L^{-1} PBS/pH 7.40 showed better stability compared to the Au/Au_{nano} electrode indicating that these modified electrodes have good reproducibility and do not suffer from surface fouling during repetitive voltammetric measurement due to Au–S bond formation.

Figure 33 showed the CV comparing the 1st, 25th, and 50th cycles of repeated cycles stability of Au/Au_{nano}–Cys electrode, I_{pa} increased from 4.9 μA in the 1st cycle up to 8.2 μA in the 25th and 50th cycles, and the oxidation peak potential shifted from 363 mV in the 1st cycle to 220 mV in the 25th and 50th cycles. This result confirms the reorganization of cysteine molecules on gold nanoparticles by repeated cycles resulting in enhanced hydrogen bond formation between EP and cysteine and improved electron transfer rate. Also, the long-term stability of Au/Au_{nano} and Au/Au_{nano}–Cys/SDS electrodes was studied for up to 1 week. I_{pa} of EP decreased by 20 % and 30 % after 3 days and 1 week of storage, respectively, in the case of Au/Au_{nano} electrode. I_{pa} decreased by 9 % and 16 % after the same periods of storage, respectively, in the case of Au/Au_{nano}–Cys/ SDS electrode. These results indicate that cysteine SAM organized on gold nanoparticles enhances the long-term stability of Au/Au_{nano}–Cys/SDS electrode due to Au–S bond formation. Therefore, Au/Au_{nano}–Cys/SDS electrode showed better stability via repeated cycles and long-term stability compared to the Au/Au_{nano} electrode [31]. In conclusion, the synergistic effect between cysteine SAM-modified gold nanoparticles and surfactant enhances the use of surfactant-modified electrodes as nanosensors with excellent reproducibility, high sensitivity, and unique selectivity.

On the other hand, Gan Yang prepared a hemoglobin (Hb)/gold colloid (nano-Au)/L-cysteine (L-cys)/nano-Au/nanoparticles Pt (nano-Pt)–chitosan (CHIT) composite film-modified Pt disk electrode as a biosensor for the determination of H_2O_2. Figure 34 compares the response of different modified electrodes toward H_2O_2. The current increased upon adsorption of L-cys on the nano-Au/nano-Pt–CHIT surface, and maximal current is obtained at the modified electrode. L-cys molecules were assembled on the nano-Au-modified electrode, and the interfacial resistance decreased as obtained from EIS study suggesting that L-cys promotes the electron transfer rate [157]. Furthermore, Guoli Shen prepared L-cysteine–gold particle nanocomposite (CGN) by a self-assembly process to involving L-cysteine on gold nanoparticles providing a general method to realize the direct electrochemistry of enzymes [138]. A new electrode interface was constructed by using CGN to be immobilized in the network of a Nafion membrane on a glassy carbon (GC) electrode (GC/NCGN). GC/NCGN was utilized to fabricate the third-generation horseradish peroxidase biosensor exhibiting good response to H_2O_2 and displayed the remarkable sensitivity and repeatability. The effect of the amount of L-cysteine on the response of the GC/NCGN was investigated. The response was rather small when only a small amount or even no L-cysteine was added to prepare the nanocomposites. This may be attributed to the formation of a rather small amount of CGN during the assembly of L-cysteine on gold nanoparticles. A maximum response was obtained when 5 μL of 10^{-3} M of L-cysteine was used, and the response decreased again when more than 5 μL of 10^{-3} M of L-cysteine was added. The optimum amount was 5 μL of 10^{-3} M of L-cysteine [138].

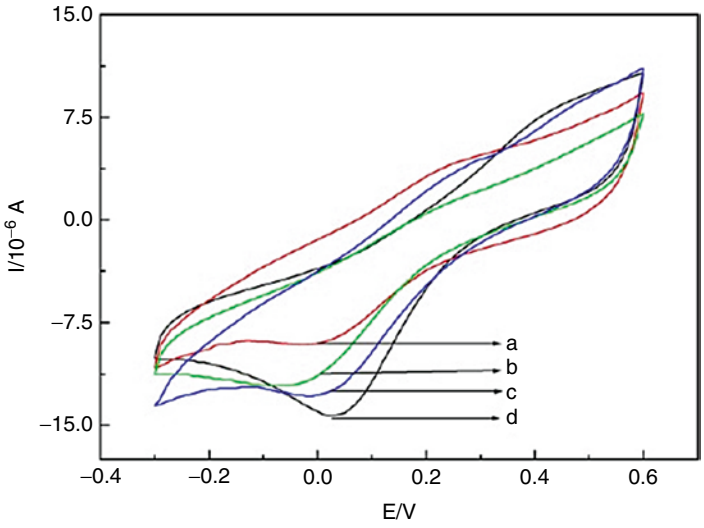

Fig. 34 Cyclic voltammograms of the different electrodes in 0.1 M pH 7.0 PBS containing 3.5×10^{-4} M H_2O_2. (*a*) Hb/n-Pt–CHIT composite film-modified Pt electrode, (*b*) Hb/n-Au/n-Pt–CHIT composite film-modified Pt electrode, (*c*) Hb/L-cys/n-Au/n-Pt–CHIT composite film-modified Pt electrode, (*d*) modified electrode (Reprinted from [157], Copyright (2008), with permission from Elsevier)

Conclusions

Self-assembled monolayer has opened up new era of exploration and has a profound impact on sensors and biosensors due to its unique properties. SAM-modified electrodes have been utilized as nanosensors with excellent reproducibility, high sensitivity, unique selectivity, and exceptional stability. Different self-assemblies were considered in this chapter: SAM of metallic nanoparticles on polymeric film, SAM of surfactant on polymeric film, and SAM of S-containing compounds on nanometallic films. Simplicity, cheapness, and fastness are the main advantages of the proposed methods utilizing SAM-modified electrodes when compared with other determination methods of different studied compounds. Furthermore, these methods are highly sensitive so that the studied analytes can be determined under physiological conditions in real urine samples with good accuracy, excellent selectivity, and sub-nanomolar concentration detection.

Acknowledgment The authors would like to recognize the Cairo University financial support that was achieved through the vice president of research funds' office.

References

1. Prakash S, Chakrabarty T, Singh AK, Shahi VK et al (2013) Polymer thin films embedded with metal nanoparticles for electrochemical biosensors applications. Biosens Bioelectron 41:43–53
2. Bello A, Giannetto M, Mori G, Seeber R, Terzi F, Zanardi C et al (2007) Optimization of the DPV potential waveform for determination of ascorbic acid on PEDOT-modified electrodes. Sens Actuators B 121:430–435
3. Lupu S (2011) In situ electrochemical preparation and characterization of PEDOT–Prussian blue composite materials. Synth Met 161:384–390
4. Pigani L, Foca G, Ionescu K, Martina V, Ulrici A, Terzi F, Vignali M, Zanardi C, Seeber R et al (2008) Amperometric sensors based on poly (3,4-ethylenedioxythiophene)-modified electrodes: discrimination of white wines. Anal Chim Acta 614:213–222
5. Istamboulie G, Sikora T, Jubete E, Ochoteco E, Marty J, Noguer T et al (2010) Screen-printed poly(3,4-ethylenedioxythiophene) (PEDOT): a new electrochemical mediator for acetylcholinesterase-based biosensors. Talanta 82:957–961
6. Ricardo A, Alves G, Ghica ME, Brett CMA et al (2011) Preparation and characterisation of poly(3,4-ethylenedioxythiophene) and poly(3,4-ethylenedioxythiophene)/poly(neutral red) modified carbon film electrodes, and application as sensors for hydrogen peroxide. Electrochim Acta 56:3685–3692
7. Atta NF, Galal A, Khalifa F et al (2007) Electrodeposited metals at conducting polymer electrodes I – effect of particle size and film thickness on electrochemical response. Appl Surf Sci 253:4273–4282
8. Selvaganesh SV, Mathiyarasu J, Phani KLN, Yegnaraman V et al (2007) Chemical synthesis of PEDOT–Au nanocomposite. Nanoscale Res Lett 2:546–549
9. Harish S, Mathiyarasu J, Phani KLN et al (2009) Generation of gold–PEDOT nanostructures at an interface between two immiscible solvents. Mater Res Bull 44:1828–1833
10. Atta NF, El-Kady MF, Galal A et al (2010) Simultaneous determination of catecholamines, uric acid and ascorbic acid at physiological levels using poly(N methylpyrrole)/Pd-nanoclusters sensor. Anal Biochem 400:78–88
11. Atta NF, El-Kady MF (2010) Novel poly(3-methylthiophene)/Pd, Pt nanoparticle sensor: synthesis, characterization and its application to the simultaneous analysis of dopamine and ascorbic acid in biological fluids. Sens Actuators B 145:299–310
12. Atta NF, El-Kady MF (2009) Poly(3-methylthiophene)/palladium sub-micro-modified sensor electrode. Part II: voltammetric and EIS studies, and analysis of catecholamine neurotransmitters, ascorbic acid and acetaminophen. Talanta 79:639–647
13. Atta NF, El-Kady MF, Galal A et al (2009) Palladium nanoclusters-coated polyfuran as a novel sensor for catecholamine neurotransmitters and paracetamol. Sens Actuators B 141: 566–574
14. Mathiyarasu J, Senthilkumar S, Phani KLN, Yegnaraman V et al (2008) PEDOT-Au nanocomposite film for electrochemical sensing. Mater Lett 62:571–573
15. Ferreira VC, Melato AI, Silva AF, Abrantes LM et al (2011) Attachment of noble metal nanoparticles to conducting polymers containing sulphur – preparation conditions for enhanced electrocatalytic activity. Electrochim Acta 56:3567–3574
16. Galal A, Atta NF, Darwish SA, Ali SM et al (2008) Electrodeposited metals at conducting polymer electrodes. II: study of the oxidation of methanol at poly(3-methylthiophene) modified with Pt–Pd Co-catalyst. Top Catal 47:73–83
17. Ferreira VC, Melato AI, Silva AF, Abrantes LM et al (2011) Conducting polymers with attached platinum nanoparticles towards the development of DNA biosensors. Electrochem Commun 13:993–996

18. Li J, Lin X (2007) Simultaneous determination of dopamine and serotonin on gold nanocluster/overoxidized-polypyrrole composite modified glassy carbon electrode. Sens Actuators B 124:486–493
19. Harish S, Mathiyarasu J, Phani KLN, Yegnaraman V et al (2008) PEDOT/palladium composite material: synthesis, characterization and application to simultaneous determination of dopamine and uric acid. J Appl Electrochem 38:1583–1588
20. Namboothiry MAG, Zimmerman T, Coldren FM, Liu J, Kim K, Carroll DL et al (2007) Electrochromic properties of conducting polymer metal nanoparticles composites. Synth Met 157:580–584
21. Kim BY, Cho MS, Kim YS, Son Y, Lee Y et al (2005) Fabrication and characterization of poly(3,4-ethylenedioxythiophene)/gold nanocomposite via in-situ redox cycle system. Synth Met 153:149–152
22. Manesh KM, Santhosh P, Gopalan A, Lee KP et al (2008) Electrocatalytic oxidation of NADH at gold nanoparticles loaded poly(3,4-ethylenedioxythiophene)–poly(styrene sulfonic acid) film modified electrode and integration of alcohol dehydrogenase for alcohol sensing. Talanta 75:1307–1314
23. Hsiao Y, Su W, Cheng J, Cheng S et al (2011) Electrochemical determination of cysteine based on conducting polymers/gold nanoparticles hybrid nanocomposites. Electrochim Acta 56:6887–6895
24. Zanardi C, Terzi F, Seeber R et al (2010) Composite electrode coatings in amperometric sensors. Effects of differently encapsulated gold nanoparticles in poly(3,4-ethylendioxythiophene) system. Sens Actuators B 148:277–282
25. Kumar SS, Mathiyarasu J, Phani KL et al (2005) Exploration of synergism between a polymer matrix and gold nanoparticles for selective determination of dopamine. J Electroanal Chem 578:95–103
26. Zanardi C, Terzi F, Pigani L, Heras A, Colina A, Lopez-Palacios J, Seeber R et al (2008) Development and characterisation of a novel composite electrode material consisting of poly(3, 4-ethylenedioxythiophene) including Au nanoparticles. Electrochim Acta 53:3916–3923
27. Atta NF, Galal A, El-Ads EH et al (2012) Gold nanoparticles-coated poly(3,4-ethylenedioxythiophene) for the selective determination of sub-nano concentrations of dopamine in presence of sodium dodecyl sulfate. Electrochim Acta 69:102–111
28. Gopalan AI, Lee K, Manesha KM, Santhosh P, Kim JH, Kang JS et al (2007) Electrochemical determination of dopamine and ascorbic acid at a novel gold nanoparticles distributed poly (4-aminothiophenol) modified electrode. Talanta 71:1774–1781
29. Bian X, Lu X, Jin E, Kong L, Zhang W, Wang C et al (2010) Fabrication of Pt/polypyrrole hybrid hollow microspheres and their application in electrochemical biosensing towards hydrogen peroxide. Talanta 81:813–818
30. Li J, Lin X (2007) Electrodeposition of gold nanoclusters on overoxidized polypyrrole film modified glassy carbon electrode and its application for the simultaneous determination of epinephrine and uric acid under coexistence of ascorbic acid. Anal Chim Acta 596:222–230
31. Atta NF, Galal A, El-Ads EH et al (2012) A novel sensor of cysteine self-assembled monolayers over gold nanoparticles for the selective determination of epinephrine in presence of sodium dodecyl sulfate. Analyst 137:2658–2668
32. Atta NF, Galal A, Ahmed RA et al (2011) Poly(3,4-ethylene-dioxythiophene) electrode for the selective determination of dopamine in presence of sodium dodecyl sulfate. Bioelectrochemistry 80:132–141
33. Nagarajan R, Ruckenstein E (1991) Theory of surfactant self -assembly: a predictive molecular thermodynamic approach. Langmuir 7:2934–2969
34. Malmsten M (2002) Surfactant and polymer in drug delivery. Marcel Dekker, New York
35. Fridrikhsberg DA (1986) A course in colloid chemistry. Mir Publishers, Moscow
36. Vittal R, Gomathi H, Kim K et al (2006) Beneficial role of surfactants in electrochemistry and in the modification of electrodes. Adv Colloid Interface Sci 119:55–68

37. Rosen MJ (1989) Surfactants and interfacial phenomena, 2nd edn. Wiley-Inter-Science, New York
38. Rusling JF (1991) Controlling electrochemical catalysis with surfactant microstructures. Acc Chem Res 24:75–81
39. Rusling JF (1994) Reactions and synthesis in surfactant systems. In: Bard AJ (ed) Electroanalytical chemistry, vol 18. Marcel Dekker, New York, p 267
40. Franklin TC, Mathew S (1989) Surfactants in solution. In: Mittall KL (ed) vol 2. Plenum, New York 267–286
41. Shinozuka N, Hayano S (1979) Solution chemistry of surfactants. In: Mitall KL (ed) vol 2. Plenum, New York
42. Diaz A, Kaifer AZ (1988) Self-assembled surfactant monolayers on electrode surfaces: the formation of surfactant viologen monolayers on Au and Pt. J Electroanal Chem 249: 333–338
43. Widrig CA, Majda M (1989) Self-assembly of ordered monolayers and bilayers of *N-methyl-N′*-octadecylviologen amphiphile on gold surfaces in aqueous solutions. Langmuir 5:639
44. Long HCD, Donohue JJ, Buttry DA et al (1991) Ionic interactions in electroactive self-assembled monolayers of ferrocene species. Langmuir 7:2196–2202
45. Grant LM, Ducker WA (1997) Effect of substrate hydrophobicity on surface – aggregate geometry: zwitterionic and nonionic surfactants. Phys Chem B 101:5337–5345
46. Grant LM, Tiberg F, Duker WA et al (1998) Nanometer-scale organization of ethylene oxide surfactants on graphite, hydrophilic silica, and hydrophobic silica. J Phys Chem B 102:4288
47. Rennie AR, Lee EM, Simister EA, Thomas RK et al (1990) Structure of a cationic surfactant layer at the silica-water interface. Langmuir 6:1031–1034
48. Manne S, Gaub HE (1995) Molecular organization of surfactants at solid–liquid interfaces. Science 270:1480–1482
49. Schulz JC, Warr GG, Bulter PD, Hamilton WA et al (2001) Adsorbed layer structure of cationic surfactants on quartz. Phys Rev E 63:041604–041608
50. Facci JS (1987) Langmuir 3:525–529
51. Rusling JF, Shi CN, Gosser DK, Shukla SS et al (1988) Electrocatalytic reactions in organized assemblies I. Reduction of 4-bromobiphenyl in cationic and nonionic micelles. J Electroanal Chem 240:201–216
52. Rusling JF (1988) Electrocatalytic systems organized by micelles. Trends Anal Chem 7:266–269
53. Boussaad S, Tao NJ (1999) Electron transfer and adsorption of myoglobin on self-assembled surfactant films: an electrochemical tapping-mode AFM study. J Am Chem Soc 121: 4510–4515
54. Liu JF, Min G, Duker WA et al (2001) AFM study of adsorption of cationic surfactants and cationic polyelectrolytes at the silica – water interface. Langmuir 17:4895
55. Retter U, Avranas A (2001) On anion-induced formation of hemicylindrical and hemispherical surface micelles of amphiphiles at the metal/electrolyte interface. Langmuir 17:5039–5044
56. Schulz JC, Warr GG (2002) Adsorbed layer structure of cationic and anionic surfactants on mineral oxide surfaces. Langmuir 18:3191–3197
57. Petri M, Kolb DM (2002) Nanostructuring of a sodium dodecyl sulfate-covered Au(111) electrode. Phys Chem 4:1211–1216
58. Wanless EJ, Duker WA (1996) Organization of sodium dodecyl sulfate at the graphite-solution interface. J Phys Chem 100:3207
59. Duker WA, Grant LM (1996) Effect of substrate hydrophobicity on surfactant surface – aggregate geometry. J Phys Chem 100:11507–11511
60. Wolgemuth JL, Workman RK, Manne S et al (2000) Surfactant aggregates at a flat, isotropic hydrophobic surface. Langmuir 16:3077–3081
61. Wanless EJ, Duker WA (1997) Weak influence of divalent ions on anionic surfactant surface-aggregation. Langmuir 13:1463–1474

62. Subramanian V, Duker WA (2000) Counterion effects on adsorbed micellar shape: experimental study of the role of polarizability and charge. Langmuir 16:4447–4454
63. Burgess I, Jeffrey CA, Cai X, Szymanski G, Lipkowski J et al (1999) Direct visualization of the potential controlled transformation of hemimicellar aggregates of dodecyl sulfate into a condensed monolayer at the electrode surface. Langmuir 15:2607–2616
64. Burgess I, Zamlynny V, Szymanski G, Lipkowski J et al (2001) Electrochemical and neutron reflectivity characterization of dodecyl sulfate adsorption and aggregation at the gold-water interface. Langmuir 17:3355–3367
65. Cholewa E, Burgess I, Kunze J et al (2004) Adsorption of *N*-dodecyl-*N*, *N*-dimethyl-3-ammonio-1-propanesulfonate (DDAPS), a model zwitterionic surfactant, on the Au(111) electrode surface. J Solid State Electrochem 8:693–705
66. Chandar P, Somasundaram P, Turro NJ et al (1987) Fluorescence probe studies on the structure of the adsorbed layer of dodecyl sulfate at the alumina – water interface. Colloid Interface Sci 117:31–46
67. Manne S (1997) Visualizing self-assembly: force microscopy of ionic surfactant aggregates at solid–liquid interfaces. Progr Colloid Polym Sci 103:226–233
68. Gao Y, Du J, Gu T et al (1987) Hemimicelle formation of cationic surfactants at silica gel–water interface. Chem Soc Faraday Trans 1:2671–2679
69. Fan A, Somasundaram P, Turro N et al (1997) Adsorption of alkyltrimethylammonium bromides on negatively charged alumina. Langmuir 13:506–510
70. Sharma BJ, Basu S, Sharma MM et al (1996) Characterization of adsorbed ionic surfactants on a mica substrate. Langmuir 12:6506–6512
71. Singh PK, Adler JJ, Rabinovich YI, Moudgil BM et al (2001) Investigation of self-assembled surfactant structures at the solid–liquid interface using FT-IR/ATR. Langmuir 17(2): 468–473
72. Li H, Tripp CP (2002) Spectroscopic identification and dynamics of adsorbed cetyltrimethylammonium bromide structures on TiO_2 surfaces. Langmuir 18:9441–9446
73. Atkin R, Craig VSJ, Wanless EJ, Biggs S et al (2003) Mechanism of cationic surfactant adsorption at the solid-aqueous interface. Adv Colloid Interface Sci 103:219–304
74. Gonzalez-Macia L, Smyth MR, Morrinb A, Killard AJ et al (2011) Enhanced electrochemical reduction of hydrogen peroxide at metallic electrodes modified with surfactant and salt. Electrochim Acta 58:562–570
75. Muray RW (1992) Molecular design of electrode surfaces, vol 22. Wiley, New York, p 18
76. Goldenberg M (1997) Use of electrochemical techniques to study the Langmuir–Blodgett films of redox active materials. Russ Chem Rev 66:1033–1052
77. Gomez M, Li J, Kaifer AE et al (1991) Surfactant monolayers on electrode surfaces: self-assembly of a series of amphiphilic viologens on gold and tin oxide. Langmuir 7:1797–1806
78. Ulman A (1991) An introduction to ultrathin organic films from Langmuir-Blodgett to self-assembly. Academic, San Diego
79. Kaifer A, Kaifer MG (1999) Supramolecular electrochemistry. Wiley-VCH, Weinheim, New York, Chichester, Brisbane, Singapore, Toronto
80. Rusling JF (1997) Molecular aspects of electron transfer at electrodes in micellar solutions. Colloids Surf 123:81–88
81. Mackay RA (1994) Electrochemistry in association colloids. Colloids Surf A 82:1–28
82. Rusling JF, Zhang H, Willis WS et al (1990) Properties of octadecylsilyl-coated electrodes in ionic micellar media. Anal Chim Acta 235:307–315
83. Guidelli R, Foresti ML (1977) The inhibitory effect of neutral organic surfactants upon simple electrode reactions. Electroanal Chem 77:73
84. Marino A, Brajter-Toth A (1993) Ionic surfactants as molecular spacers at graphite electrodes. Anal Chem 65:370–374
85. Lee KAB (1990) Electron transfer into self-assembling monolayers on gold electrodes. Langmuir 6:709–712
86. Chidsey CED (1991) Free energy and temperature dependence of electron transfer at the metal-electrolyte interface. Science 251:919–922

87. Abbott AP, Gounili G, Bobbitt JM, Rusling JF, Kumosinski TF et al (1992) Electron transfer between amphiphilic ferrocenes and electrodes in cationic micellar solution. J Phys Chem 96:11091–11095
88. Marcus RA (1964) Chemical and electrochemical electron-transfer theory. Annu Rev Phys Chem 15:155–196
89. Georges J, Desmettre S (1984) Electrochemistry of ferrocene in anionic, cationic and non-ionic micellar solutions. Effect of the micelle solubilization of the half-wave potentials. Electrochim Acta 29:521–525
90. Fendler JH (1982) Membrane mimetic chemistry. Wiley, New York
91. Hosseinzadeh R, Sabzi RE, Ghasemlu K et al (2009) Effect of cetyltrimethyl ammonium bromide (CTAB) in determination of dopamine and ascorbic acid using carbon paste electrode modified with tin hexacyanoferrate. Colloids Surf B 68:213–217
92. Paria S, Khilar KC (2004) A review on experimental studies of surfactant adsorption at the hydrophilic solid–water interface. Adv Colloid Interface Sci 110:75–95
93. Love LJC, Habarta JG, Dorsey JG et al (1984) The micelle-analytical chemistry interface. Anal Chem 56:1132A–1148A
94. Yang C, Sang Q, Zhang S, Huang W et al (2009) Voltammetric determination of estrone based on the enhancement effect of surfactant and a MWNT film electrode. Mater Sci Eng C 29:1741–1745
95. Hu C, Yang C, Hu S et al (2007) Hydrophobic adsorption of surfactants on water-soluble carbon nanotubes: a simple approach to improve sensitivity and antifouling capacity of carbon nanotubes-based electrochemical sensors. Electrochem Commun 9:128–134
96. Jain R, Mishra R, Dwivedi A et al (2009) Effect of surfactant on voltammetric behaviour of ornidazole. Colloids Surf A 337:74–79
97. Liu S, Li J, Zhang S, Zhao J et al (2005) Study on the adsorptive stripping voltammetric determination of trace cerium at a carbon paste electrode modified in situ with cetyltrimethylammonium bromide. Appl Surf Sci 252:2078
98. Svancara I, Foret P, Vytras K et al (2004) A study on the determination of chromium as chromate at a carbon paste electrode modified with surfactants. Talanta 64:844–852
99. Hoyer B, Jensen N (2004) Use of sodium dodecyl sulfate as an antifouling and homogenizing agent in the direct determination of heavy metals by anodic stripping voltammetry. Analyst 129:751–754
100. Dar RA, Brahman PK, Tiwari S, Pitre KS et al (2012) Electrochemical studies of quinine in surfactant media using hanging mercury drop electrode: a cyclic voltammetric study. Colloids Surf B 98:72–79
101. Atta NF, Galal A, Ahmed RA et al (2011) Simultaneous determination of catecholamines and serotonin on poly(3,4-ethylene dioxythiophene) modified Pt electrode in presence of sodium dodecyl sulfate. J Electrochem Soc 158(4):F52–F60
102. Atta NF, Galal A, Abu-Attia FM, Azab SM et al (2011) Characterization and electrochemical investigations of micellar/drug interactions. Electrochim Acta 56:2510–2517
103. Castilho M, Almeida LE, Tabak M, Mazo LH et al (2000) The electrochemical oxidation of the antioxidant drug dipyridamole at glassy carbon and graphite electrodes in micellar solutions. Electrochim Acta 46:67–75
104. Goyal RN, Jain N, Gurnani V et al (2001) Electrooxidation of chlorpromazine in aqueous and micellar media and spectroscopic studies of the derived cationic free radical and dication species. Monatsh Chem 132:575–585
105. Wang LH, Tseng SW (2001) Direct determination of D-panthenol and salt of pantothenic acid in cosmetic and pharmaceutical preparations by differential pulse voltammetry. Anal Chim Acta 432:39–48
106. Zhang S, Wu K, Hu S et al (2002) Voltammetric determination of diethylstilbestrol at carbon paste electrode using cetylpyridine bromide as medium. Talanta 58:747–754
107. Zhang S, Wu K, Hu S et al (2002) Carbon paste electrode based on surface activation for trace adriamycin determination by a preconcentration and voltammetric method. Anal Sci 18: 1089–1092

108. Fernandez SG, Lopez MCB, Castanon MJL, Ordieres AJM, Blanco PT et al (2004) Adsorptive stripping voltammetry of rifamycins at unmodified and surfactant-modified carbon paste electrodes. Electroanalysis 16:1660–1666
109. Atta NF, Galal A, Ahmed RA et al (2011) Direct and simple electrochemical determination of morphine at PEDOT modified Pt electrode. Electroanalysis 23(3):737–746
110. Atta NF, Galal A, Ahmed RA et al (2011) Voltammetric behavior and determination of isoniazid using PEDOT electrode in presence of surface active agents. Int J Electrochem Sci 6:5097–5113
111. Brahman PK, Dar RA, Tiwari S, Pitre KS et al (2012) Voltammetric determination of anticancer drug flutamide in surfactant media at polymer film modified carbon paste electrode. Colloids Surf A 396:8–15
112. Li C, Ya Y, Zhan G et al (2010) Electrochemical investigation of tryptophan at gold nanoparticles modified electrode in the presence of sodium dodecylbenzene sulfonate. Colloids Surf B 76:340–345
113. Yang G, Qu X, Shen M, Wang C, Qu Q, Hu X et al (2007) Preparation of glassy carbon electrode modified by hydrophobic gold nanoparticles and its application for the determination of ethamsylate in the presence of cetyltrimethylammonium bromide. Sens Actuators B 128:258–265
114. Chaki NK, Vijayamohanan K (2002) Self-assembled monolayers as a tunable platform for biosensor applications. Biosens Bioelectron 17:1–12
115. Park B, Yoon D, Kim D et al (2011) Formation and modification of a binary self-assembled monolayer on a nano-structured gold electrode and its structural characterization by electrochemical impedance spectroscopy. J Electroanal Chem 661(2):329–335
116. Goldmann M, Davidovits JV, Silberzan P et al (1998) Kinetics of self-assembled silane monolayers at various temperatures: evidence of 2D foam. Thin Solid Films 327–329: 166–171
117. Maksymovych P, Voznyy O, Dougherty DB, Sorescu DC, Yates JT Jr et al (2010) Gold adatom as a key structural component in self-assembled monolayers of organosulfur molecules on Au(111). Prog Surf Sci 85:206–240
118. Campuzano S, Pedrero M, Montemayor C, Fatàs E, Pingarrón JM et al (2006) Characterization of alkanethiol-self-assembled monolayers-modified gold electrodes by electrochemical impedance spectroscopy. J Electroanal Chem 586:112–121
119. Ozoemena KI, Nyokong T (2006) Comparative electrochemistry and electrocatalytic activities of cobalt, iron and manganese phthalocyanine complexes axially co-ordinated to mercaptopyridine self-assembled monolayer at gold electrodes. Electrochim Acta 51: 2669–2677
120. Xian Y, Wang H, Zhou Y, Pan D, Liu F, Jin L et al (2004) Preparation of L-Cys–Au colloid self-assembled nanoarray electrode based on the microporous aluminium anodic oxide film and its application to the measurement of dopamine. Electrochem Commun 6:1270–1275
121. Freire RS, Kubota LT (2004) Application of self-assembled monolayer-based electrode for voltammetric determination of copper. Electrochim Acta 49:3795–3800
122. Wang T, Bai Y, Luo H, Yan X, Zheng W et al (2011) Electrochemical characteristic of selenocysteine self-assembly monolayers at Au electrode. J Electroanal Chem 657:74–78
123. Desikan R, Lee I, Thundat T et al (2006) Effect of nanometer surface morphology on surface stress and adsorption kinetics of alkanethiol self-assembled monolayers. Ultramicroscopy 106:795–799
124. Krysiński P, Brzostowska-Smolska M (1998) Capacitance characteristics of self-assembled monolayers on gold electrode. Bioelectrochem Bioenerg 44:163–168
125. Sun J, Xu J, Fang H, Chen H et al (1997) Electrocatalytic oxidation of NADH with dopamine covalently bound to self-assembled cysteamine monolayers on gold electrode. Bioelectrochem Bioenerg 44:45–50
126. Zhao YQ, Luo HQ, Li NB et al (2009) Electrochemical characterization of in situ functionalized gold *p*-aminothiophenol self-assembled monolayer with 4-formylphenylboronic acid for recognition of sugars. Sens Actuators B 137:722–726

127. Kühnle A (2009) Self-assembly of organic molecules at metal surfaces. Curr Opin Colloid Interface Sci 14:157–168
128. Lang P, Nogues C (2008) Self-assembled alkanethiol monolayers on a Zn substrate: interface studied by XPS. Surf Sci 602:2137–2147
129. Zhang H, Li N, Zhu Z et al (2000) Electrocatalytic response of dopamine at a DL-HOMOCYSTEINE self-assembled gold electrode. Microchem J 64:277–282
130. Duwez A (2004) Exploiting electron spectroscopies to probe the structure and organization of self-assembled monolayers: a review. J Electron Spectrosc Relat Phenom 134:97–138
131. Briand E, Salmain M, Compére C, Pradier C et al (2006) Immobilization of protein a on SAMs for the elaboration of immunosensors. Colloids Surf B 53:215–224
132. Arezki B, Delcorte A, Bertrand P et al (2004) Emission processes of molecule–metal cluster ions from self-assembled monolayers of octanethiols on gold and silver. Appl Surf Sci 231:122–126
133. Saga Y, Tamiaki H (2004) Facile synthesis of chlorophyll analog possessing a disulfide bond and formation of self-assembled monolayer on gold surface. J Photochem Photobiol B 73:29–34
134. Behera S, Raj CR (2007) Self-assembled monolayers of thio-substituted nucleobases on gold electrode for the electroanalysis of NADH, ethanol and uric acid. Sens Actuators B 128: 31–38
135. Zhang X, Wang S (2005) Determination of ethamsylate in the presence of catecholamines using 4-amino-2-mercaptopyrimidine self-assembled monolayer gold electrode. Sens Actuators B 104:29–34
136. Zhong X, Yuan R, Chai Y, Liu Y, Dai J, Tang D et al (2005) Glucose biosensor based on self-assembled gold nanoparticles and double-layer 2d-network (3-mercaptopropyl)-trimethoxysilane polymer onto gold substrate. Sens Actuators B 104:191–198
137. Raj CR, Ohsaka T (2003) Voltammetric detection of uric acid in the presence of ascorbic acid at a gold electrode modified with a self-assembled monolayer of heteroaromatic thiol. J Electroanal Chem 540:69–77
138. Li X, Wu J, Gao N, Shen G, Yu R et al (2006) Electrochemical performance of L-cysteine–gold particle nanocomposite electrode interface as applied to preparation of mediator-free enzymatic biosensors. Sens Actuators B 117:35–42
139. Liu Z, He Q, Xiao P, Liang B, Tan J, He N, Lu Z et al (2003) Self-assembly monolayer of mercaptopropyltrimethoxysilane for electroless deposition of Ag. Mater Chem Phys 82:301–305
140. Hoffmann H, Mayer U, Brunner H, Krischanitz A et al (1995) Reflection-absorption infrared spectroscopy of self-assembled monolayers on gold and silicon surfaces. Vib Spectrosc 8: 151–157
141. Wang S, Du D (2002) Studies on the electrochemical behaviour of hydroquinone at L-cysteine self-assembled monolayers modified gold electrode. Sensors 2:41–49
142. Giz MJ, Duong B, Tao NJ et al (1999) In situ STM study of self-assembled mercaptopropionic acid monolayers for electrochemical detection of dopamine. J Electroanal Chem 465:72–79
143. Dodero G, Michieli LD, Cavalleri O, Rolandi R, Oliveri L, Daccà A, Parodi R et al (2000) L-Cysteine chemisorption on gold: an XPS and STM study. Colloids Surf A 175:121–128
144. Wang Q, Dong D, Li N et al (2001) Electrochemical response of dopamine at a penicillamine self-assembled gold electrode. Bioelectrochemistry 54:169–175
145. Wang Q, Jiang N, Li N et al (2001) Electrocatalytic response of dopamine at a thiolactic acid self-assembled gold electrode. Microchem J 68:77–85
146. Li J, Cheng G, Dong S et al (1997) Electrochemical study of the interfacial characteristics of redox-active viologen thiol self-assembled monolayers. Thin Solid Films 293:200–205
147. Łuczak T (2009) Comparison of electrochemical oxidation of epinephrine in the presence of interfering ascorbic and uric acids on gold electrodes modified with S-functionalized compounds and gold nanoparticles. Electrochim Acta 54:5863–5870
148. Shervedani RK, Bagherzadeh M, Mozaffari SA et al (2006) Determination of dopamine in the presence of high concentration of ascorbic acid by using gold cysteamine self-assembled monolayers as a nanosensor. Sens Actuators B 115:614–621

149. Zhuo Y, Yu R, Yuan R, Chai Y, Hong C et al (2009) Enhancement of carcinoembryonic antibody immobilization on gold electrode modified by gold nanoparticles and SiO_2/Thionine nanocomposite. J Electroanal Chem 628:90–96
150. El-Deab MS, Ohsaka T (2003) Quasi-reversible two-electron reduction of oxygen at gold electrodes modified with a self-assembled submonolayer of cysteine. Electrochem Commun 5:214–219
151. Raj CR, Ohsaka T (2001) Electroanalysis of ascorbate and dopamine at a gold electrode modified with a positively charged self-assembled monolayer. J Electroanal Chem 496: 44–49
152. Liu T, Li M, Li Q et al (2004) Electroanalysis of dopamine at a gold electrode modified with *N*-acetylcysteine self-assembled monolayer. Talanta 63:1053–1059
153. Dalmia A, Liu CC, Savinell RF et al (1997) Electrochemical behavior of gold electrodes modified with self-assembled monolayers with an acidic end group for selective determination of dopamine. J Electroanal Chem 430:205–214
154. Aryal S, Dharmaraj N, Bhattarai N, Kim CH, Kim HY et al (2006) Spectroscopic identification of S Au interaction in cysteine capped gold nanoparticles. Spectrochim Acta A 63:160–163
155. Liu S, Li X, Li Y, Li Y, Li J, Jiang L et al (2005) The influence of gold nanoparticle modified electrode on the structure of mercaptopropionic acid self-assembly monolayer. Electrochim Acta 51:427–431
156. Galal A, Atta NF, El-Ads EH et al (2012) Probing cysteine self-assembled monolayers over gold nanoparticles – towards selective electrochemical sensors. Talanta 93:264–273
157. Yang G, Yuan R, Chai Y et al (2008) A high-sensitive amperometric hydrogen peroxide biosensor based on the immobilization of hemoglobin on gold colloid/L-cysteine/gold colloid/nanoparticles Pt–chitosan composite film-modified platinum disk electrode. Colloids Surf B 61:93–100